

May 2018

# Primordial Black Holes in the Cosmological Context and Transient Electromagnetic Signatures from Merging Black Hole Binaries

Jared Robert Rice  
jared.r.rice@gmail.com

Follow this and additional works at: <https://digitalscholarship.unlv.edu/thesesdissertations>



Part of the [Astrophysics and Astronomy Commons](#)

---

## Repository Citation

Rice, Jared Robert, "Primordial Black Holes in the Cosmological Context and Transient Electromagnetic Signatures from Merging Black Hole Binaries" (2018). *UNLV Theses, Dissertations, Professional Papers, and Capstones*. 3318.

<https://digitalscholarship.unlv.edu/thesesdissertations/3318>

This Dissertation is protected by copyright and/or related rights. It has been brought to you by Digital Scholarship@UNLV with permission from the rights-holder(s). You are free to use this Dissertation in any way that is permitted by the copyright and related rights legislation that applies to your use. For other uses you need to obtain permission from the rights-holder(s) directly, unless additional rights are indicated by a Creative Commons license in the record and/or on the work itself.

This Dissertation has been accepted for inclusion in UNLV Theses, Dissertations, Professional Papers, and Capstones by an authorized administrator of Digital Scholarship@UNLV. For more information, please contact [digitalscholarship@unlv.edu](mailto:digitalscholarship@unlv.edu).

PRIMORDIAL BLACK HOLES IN THE COSMOLOGICAL CONTEXT  
AND TRANSIENT ELECTROMAGNETIC SIGNATURES  
FROM MERGING BLACK HOLE BINARIES

by

Jared Robert Rice

Bachelor of Science – Physics (Astrophysics)  
University of California, Santa Cruz  
2008

Master of Science – Physics  
Montana State University  
2012

A dissertation submitted in partial fulfillment  
of the requirements for the

Doctor of Philosophy – Astronomy

Department of Physics and Astronomy  
College of Sciences  
The Graduate College

University of Nevada, Las Vegas  
May 2018



This work is licensed under the Creative Commons Attribution-NonCommercial-ShareAlike 4.0 International License. To view a copy of this license, visit <https://creativecommons.org/licenses/by-nc-sa/4.0/> or send a letter to

Creative Commons  
PO Box 1866  
Mountain View, CA 94042  
USA.

**Dissertation Approval**

The Graduate College  
The University of Nevada, Las Vegas

April 6, 2018

This dissertation prepared by

Jared Robert Rice

entitled

Primordial Black Holes in the Cosmological Context and Transient Electromagnetic  
Signatures from Merging Black Hole Binaries

is approved in partial fulfillment of the requirements for the degree of

Doctor of Philosophy - Astronomy  
Department of Physics and Astronomy

Bing Zhang, Ph.D.  
*Examination Committee Chair*

Kathryn Hausbeck Korgan, Ph.D.  
*Graduate College Interim Dean*

Stephen Lepp, Ph.D.  
*Examination Committee Member*

Jason Steffen, Ph.D.  
*Examination Committee Member*

Darrell Pepper, Ph.D.  
*Graduate College Faculty Representative*

# Abstract

## PRIMORDIAL BLACK HOLES IN THE COSMOLOGICAL CONTEXT AND TRANSIENT ELECTROMAGNETIC SIGNATURES FROM MERGING BLACK HOLE BINARIES

by

Jared Robert Rice

Dr. Bing Zhang, Examination Committee Chair  
Professor of Astrophysics  
University of Nevada, Las Vegas

The cosmological evolution of primordial black holes (PBHs) is presented via analysis of the accretion and evaporation histories of the holes. The ultimate end of any BH is evaporation — a spectacular seconds-long burst of high-energy radiation and particles. The critical initial mass of a PBH undergoing current era evaporation is  $\sim 510$  trillion grams. A near-critical mass PBH will not accrete radiation or matter in sufficient quantity to retard its inevitable evaporation, if the hole remains within an average volume of the universe. The gravitational waves (GWs) from five BH binary merger events discovered by the LIGO/Virgo collaborations were BHs of a few to tens of solar masses merging at redshift  $z \sim 0.1$ . It is plausible these systems began as PBHs within overdense regions of the Universe. However, it is difficult for isolated PBHs to become supermassive black holes (SMBHs) at high redshift.

A new type of electromagnetic (EM) counterpart is presented. During the inspiral of

a SMBH binary system, copious amounts of GW and EM energy are injected into the surrounding interstellar medium. The injected EM energy produces a relativistic blastwave, which emits synchrotron radiation in a transient multiwavelength afterglow. A simultaneous detection of the GWs and afterglow emission will contribute insights into blastwave dynamics, the BH masses and angular momenta, and the inner galactic environment.

# Acknowledgements

I love these wonderful human beings whose presence completes the structure of my being. There are many to thank, not the very least you, the reader. This work was partially supported by the Nevada NASA Space Grant College and Fellowship Training Program Cooperative Agreement #NNX10AN23H and I am grateful for the support.

I want to thank the members of my graduate committee: Stephen Lepp, Jason Steffen, Darrell Pepper, and my advisor Bing Zhang. Thank you for keeping me on track to graduate and encouraging my success. Thank you also to Robert Zavala in Flagstaff – you are the best unofficial co-advisor and I look forward to continuing our collaboration.

I could not have completed this dissertation without the constant and wonderful support of my friends. To my fellow graduate students here in Las Vegas: Greg Colarch, John Boisvert, Sandamali Weerasooriya, Divya Palaniswamy, and Ye Li – it was a pleasure of mine to study astrophysics alongside such brilliant minds. Your friendship was and is an integral part of my existence here at UNLV. Thank you also to Natasa Korceba for your unwavering support. I will miss our long conversations. To my friends Belinda, Alexis, Mazel, Lisa, and Ron: thank you for all of the love and support over the last five years. To Tobi, Tom, and Rori: thank you for welcoming us into your home so many times over the years. We are grateful to have you in our lives. To Bruce and Viki: thank you for all the good times. “What about the Moon, man!?”

To Carolina and Joe at CAPS: I cannot express enough how thankful I am for your continuing support. I will continue to practice mindfulness every day for the rest of my life.

Thank you for introducing me to a world of support I never knew existed.

To my friends Aaron and Shane in Montana: I could not have found a more interesting, loving, and hilarious set of friends if I tried. You kept me sane in Montana and have been a beacon of light in my life for nearly a decade now. Thank you for everything.

To Gary and Dawn: thank you for all you have done for Jocelyn and me. Our bike rides, hikes, and dinner conversations have significantly improved our lives here in Las Vegas. Thank you for always supporting my career as an astrophysicist. I am honored to be in your company. Let's do dinner again sometime soon.

To my advisor Bing: I could not have completed this dissertation without your patient support and friendship. When I asked to be your student you made no hesitation in taking me in, and for that I am eternally grateful. Thank you for your insights, discussions, and kindness. I cannot wait to see where our collaboration takes us.

To my brother, Justin: thank you for being in my life and always engaging me in interesting and awesome conversations. Thank you for being the best older brother a guy could ask for – I hope we can spend some time together this summer in the mountains! Love you, Bro!

To Mom and Dad: I am not sure there are words to describe how blessed I am to have you as my parents. Thank you for every loving sacrifice you made to bring me to this point. You were always there cheering me on, through every good day and bad. If I could give you a doctorate in parenting I would. I love you.

To my wife, Jocelyn: you are the fire in my heart that keeps me going. I could not have finished this dissertation without your unconditional love. I am proud to call you my wife. I think God had a great time when He created you — He sprinkled so much brilliance, beauty, and love into one human that I am reminded every day of how lucky I am to be your husband. You complete me in every way. I love you.

# Dedication

For Mom, Dad, and Jocelyn

# Contents

Abstract	iii
Acknowledgements	v
Dedication	vii
List of Tables	x
List of Figures	xi
<b>1 Introduction</b>	<b>1</b>
1.1 Primordial black holes	2
1.2 Electromagnetic counterparts of binary black hole mergers	2
<b>2 PBH evaporation and accretion</b>	<b>4</b>
2.1 Introduction	5
2.2 Cosmological model	6
2.3 Primordial black hole accretion and evaporation	12
2.3.1 Late universe accretion	16
2.3.2 Post-recombination accretion	19
2.3.3 Pre-recombination accretion	20
2.3.4 Post-DM freeze-out accretion	23
2.3.5 Pre-DM freeze-out accretion	24
2.4 Results	25
2.5 Conclusions and Discussion	30
<b>3 Transient electromagnetic signature of SMBHB mergers</b>	<b>34</b>
3.1 Special relativity	35
3.2 General relativity and gravitational waves	37
3.2.1 GWs from compact binary coalescence	45
3.2.2 Electromagnetic counterparts of binary black hole mergers	49
3.3 Blastwave afterglow synchrotron emission	50
<b>A Maximum PBH formation mass</b>	<b>61</b>
<b>B Sound speed in the cosmological fluid</b>	<b>62</b>

C Gravitational wave luminosity	65
References	68
Curriculum Vitae	74

# List of Tables

2.1	Standard model elementary particles and other mass thresholds important in the early universe. . . . .	9
2.2	Properties of the universe across a large range in redshift. . . . .	25
2.3	PBH accretion and evaporation properties across a large range in redshift. . . . .	26

# List of Figures

2.1	Stepwise approximation of $g_*$ as a function of temperature, including only relativistic particles whose number density is high enough to contribute. . . .	10
2.2	Waterfall plot of various PBHs forming at $z = 10^{16}$ with masses near the critical evaporation mass, $M_{cr} \sim 5.1 \times 10^{14}$ g. . . . .	27
2.3	Look-up plot of the final mass of PBHs forming at 1.0 s after the Big Bang and ending at redshifts 30, 6, 0.1, and $10^{-4}$ . . . . .	28
2.4	Full look-up plot for all PBHs forming at 1.0 s after the Big Bang and ending at redshifts 30, 6, 0.1, and $10^{-4}$ ; same color scheme as Fig. 2.3. . . . .	29
3.1	Non-spinning equal mass $10^8 M_\odot$ SMBHB coalescence time domain gravitational wave strain. . . . .	57
3.2	Non-spinning equal mass $10^8 M_\odot$ SMBHB coalescence frequency evolution. . . . .	58
3.3	Non-spinning equal mass $10^8 M_\odot$ SMBHB coalescence dimensionless orbital velocity. . . . .	59
3.4	Non-spinning equal mass $10^8 M_\odot$ SMBHB coalescence GW phase. . . . .	60
B.1	Plot of sound speed in the baryonic gas against redshift. . . . .	64

# Chapter 1

## Introduction

Albert Einstein elucidated the nature of gravity as geometry one hundred and two years ago [1, 2, 3, 4, 5]. Fifty years prior, James Clerk Maxwell established that “...light is an electromagnetic disturbance propagated through the field according to electromagnetic laws [6],” a fact corroborated by Einstein in his discovery of special relativity [7]. One year after Einstein’s gravitational revelations, Karl Schwarzschild solved the Einstein field equations for a static spherically symmetric mass [8]. Schwarzschild’s solution was critical in the study of spacetime singularities, the particular brand of which became known as “black holes.” Stephen Hawking postulated the particle emission rate from a Schwarzschild black hole by combining the formalisms of general relativity (GR) and quantum field theory (QFT) [9]. Black holes, with their large energy density, and propensity toward evolution via particle emission or accretion, maintain a provocative position as arbiter of both gravitational and electromagnetic information. This dissertation explores various aspects of gravity and electromagnetism in the context of primordial black holes and electromagnetic counterparts of binary black hole merger events in the cosmological context. The contents of Chapter 2 are published in the paper “Cosmological evolution of primordial black holes” [10] and the contents of Chapter 3 will be submitted for publication soon [11].

## 1.1 Primordial black holes

Primordial black holes (PBHs) are black holes that may have formed within the first moments of the universe through a variety of mechanisms. Fifty-two years ago, Zel'dovich and Novikov postulated the existence of these holes in a remarkable paper [12], placing constraints on the PBH number density from cosmic microwave background (CMB) observations.

In the half-Century following this prediction, PBHs have yet to be discovered. However, the various constraints on their existence are much tighter [13] and potential PBH burst signals have been investigated [14]. Prospects for discovering evidence of PBHs are encouraging, but a non-discovery is also important and will place interesting constraints on conditions in the early universe.

## 1.2 Electromagnetic counterparts of binary black hole mergers

The discovery of gravitational waves from a merging black hole binary system GW150914 [15] opened a gravitational window on the universe. We now live in the era of gravitational wave astronomy. Subsequent discoveries of the black hole merger systems GW151226, GW170104, GW170608, and GW170814 [16, 17, 18, 19] have placed important constraints on the event rate of BHB mergers, black hole binary formation channels, and cosmological models.

Four days prior to the Great American Eclipse of August 21, 2017, the LIGO/Virgo team announced the discovery of GWs from a neutron star binary merger, followed by a gamma-ray trigger on the Fermi and INTEGRAL satellites  $\sim 1.7$  s after the merger [15]. The dual detection of GWs and electromagnetic signals, combined with a fortuitous sky location that prevented Virgo from detecting a signal [20], provided a small target localization of  $\sim 30$  deg<sup>2</sup> and allowed teams of astronomers around the world to narrow down the source to within a particular galaxy, NGC 4993. With this incredible discovery, we now reside in the era of

multimessenger gravitational wave astronomy.

The purpose of this dissertation is to explore some aspects of PBHs and separately, electromagnetic counterparts of black hole binary coalescence events.

# Chapter 2

## PBH evaporation and accretion

The cosmological evolution of primordial black holes (PBHs) is considered. A comprehensive view of the accretion and evaporation histories of PBHs across the entire cosmic history is presented, with focus on the critical mass holes. The critical mass of a PBH for current era evaporation is  $M_{cr} \sim 5.1 \times 10^{14}$  g. Across cosmic time such a black hole will not accrete radiation or matter in sufficient quantity to retard the inevitable evaporation, if the black hole remains within an average volume of the universe. The accretion rate onto PBHs is most sensitive to the mass of the hole, the sound speed in the cosmological fluid, and the energy density of the accreted components. It is not easy for a PBH to accrete the average cosmological fluid to reach  $30M_{\odot}$  by  $z \sim 0.1$ , the approximate mass and redshift of the merging BHs that were the sources of the gravitational wave events GW150914 and GW151226. A PBH located in an overdense region can undergo enhanced accretion leading to the possibility of growing by many orders of magnitude across cosmic history. Thus, two merging PBHs are a plausible source for the observed gravitational wave events. However, it is difficult for isolated PBHs to grow to supermassive black holes (SMBHs) at high redshift with masses large enough to fit observational constraints.

## 2.1 Introduction

Primordial black holes (PBHs) are among the most intriguing ghosts in the universe. A singular PBH of sufficient mass can navigate the history of the universe without detectable clues to its existence; a true cosmic ghost. Low mass PBHs evaporate before the current epoch and the radiation signature of an isolated high mass PBH is too weak to detect. The last moments of a PBH evaporation reveal the hole through a burst of high-energy radiation that is distinguishable from that of short gamma-ray bursts (GRBs) [14].

The upper limits on the number density of PBHs across a wide range of masses is discussed extensively in [13, 21]. To date there are no confirmed PBH burst signals, but these compelling ghosts are ripe cosmological messengers that will enhance our understanding of the universe if observed. The PBHs evolving through cosmic history could be used as a proxy for understanding the conditions in the early universe. PBHs of significant mass may gain a dark matter (DM) halo, e.g. [22, 23]. Since the PBH evaporation rate depends only on the mass of the hole and the assumed particle physics model [24], PBHs in similar astrophysical environments should produce similar radiation signatures; the ultimate “standard candles.”

This study explores the evolution of PBHs through accretion and evaporation across the entire cosmic history. Special attention is paid to the changes in the density, temperature, and sound speed in the cosmological fluid because of their influence on the accretion rate of that fluid onto the PBHs. In §2.2 the concordance cosmological model of  $\Lambda$ CDM is discussed. In §2.3 the PBH accretion and evaporation models are discussed and formulae are given for the accretion rates in the various cosmological eras. In §2.4 the results of the study are discussed. Finally in §2.5 the conclusions are presented and a discussion of astrophysical implications is made.

## 2.2 Cosmological model

The concordance cosmology assumed throughout this study is the six parameter  $\Lambda$ CDM model, implementing the most recent *Planck* Collaboration results [25]. The model consists of the homogeneous and isotropic Friedmann-Robertson-Walker (FRW) geometry dynamically evolving according to the Einstein field equations. The Einstein equations, also called the Friedmann equations [26, 27] in this case, describe the evolution of the curvature and energy content of the universe as

$$\left(\frac{\dot{a}}{a}\right)^2 + \frac{kc^2}{a^2} = \frac{8\pi G}{3}\rho, \quad (2.1)$$

$$\frac{\ddot{a}}{a} = -\frac{4\pi G}{3}\left(\rho + \frac{3P}{c^2}\right), \quad (2.2)$$

$$\frac{d}{dt}(\rho a^3) = -\frac{P}{c^2}\frac{d}{dt}(a^3), \quad (2.3)$$

where the scale factor is  $a \equiv a_0(1+z)^{-1}$ , with the scale factor today  $a_0 \equiv 1$  and  $z$  the cosmological redshift,  $k = 0, \pm 1$  indicating zero, positive, or negative spatial curvature respectively,  $G$  is the universal gravitation constant, and  $c$  is the speed of light. The term  $\rho$  is the sum of the proper inertial mass densities of the cosmological fluid and the contribution from spatial curvature, and  $P$  is the pressure contribution from matter, radiation, and vacuum energy (or cosmological constant  $\Lambda$ ).

The equation of state of each cosmological fluid can be expressed  $P_i = w_i \rho_i c^2$  (no sum over  $i$ ) with equation of state parameter  $w_i$ . The equation of state parameters for matter, radiation, cosmological constant, and spatial curvature are 0, 1/3,  $-1$ , and  $-1/3$  respectively. Note that the equation of state of a baryonic gas  $P \propto \rho^\gamma$ , where  $\gamma$  is the adiabatic index, is relevant when calculating accretion rates onto a compact object. The approximation  $w_{i=b} \approx 0$  for a baryonic gas holds on cosmological scales.

The Hubble parameter  $H$  is a measure of the temporal (extrinsic) curvature of the FRW

geometry and is defined

$$\left(\frac{\dot{a}}{a}\right)^2 \equiv H^2 = H_0^2 \mathcal{E}^2, \quad (2.4)$$

where subscript-0 implies evaluation of a quantity today. The Hubble constant is  $H_0 = 100h \text{ km s}^{-1}\text{Mpc}^{-1}$  where the dimensionless Hubble parameter is  $h = 0.6774$  from *Planck* [25]. Before defining  $\mathcal{E}^2$ , it is convenient to introduce the dimensionless density parameters today

$$\Omega_{i,0} \equiv \frac{\rho_{i,0}}{\rho_{cr,0}} = \frac{8\pi G}{3H_0^2} \rho_{i,0}, \quad (2.5)$$

where  $i$  indicates baryonic matter, dark matter, radiation, and  $\Lambda$ . Dividing Eq. (2.1) by  $H^2$  and evaluating the quantities today gives an expression for the ‘effective’ dimensionless density parameter for spatial curvature

$$\Omega_{k,0} = 1 - \Omega_0, \quad (2.6)$$

where  $\Omega_0 \equiv \Omega_{r,0} + \Omega_{m,0} + \Omega_{\Lambda,0}$ . The combined *Planck* and baryon acoustic oscillation data [25] are consistent with  $\Omega_{k,0} = 0.000 \pm 0.005$ , i.e. the universe has zero spatial curvature to within 0.5% accuracy. The term  $\mathcal{E}^2$  in Eq. (2.4) is a function of the dimensionless density parameters with their redshift dependencies

$$\begin{aligned} \mathcal{E}^2 &\equiv \sum_i \Omega_{i,0} (1+z)^{3(1+w_i)} \\ &= \Omega_{r,0} (1+z)^4 + \Omega_{m,0} (1+z)^3 \\ &\quad + (1 - \Omega_0) (1+z)^2 + \Omega_{\Lambda,0}. \end{aligned} \quad (2.7)$$

In the FRW geometry, proper time is related to redshift through the differential  $\dot{z} = -H(z)(1+z)$ . Therefore the time  $\Delta t \equiv t_2 - t_1$  elapsed between any two redshifts  $z_1$  and  $z_2$

is given by the integral

$$\Delta t \equiv \int_{t_1}^{t_2} dt = H_0^{-1} \int_{z_2}^{z_1} \frac{dz}{(1+z)\mathcal{E}(z)}, \quad (2.8)$$

which has no tractable analytic solution ordinarily, but may be calculated analytically in simple cases or numerically in general. The age of the universe calculated numerically from Eq. (2.8) is  $t_0 = 13.8$  Gyr, which was reported in the 2015 *Planck* results [25].

The spatially-averaged inertial mass densities of the various components of the cosmological fluid decrease as power-laws with decreasing redshift according to their equation of state, i.e.

$$\rho_i \propto (1+z)^{3(1+w_i)} \quad (2.9)$$

for matter, radiation, curvature, and the cosmological constant. The average matter density in the universe evolves as  $\rho_m \propto (1+z)^3$ . The effective mass density of radiation evolves as  $\rho_r \propto (1+z)^4$ . In the early universe the redshift dependence of this term is more complicated due to the presence of radiation in the form of neutrinos and other relativistic Standard Model (SM) particles in addition to photons. Thus  $\rho_r$  evolves [28, 29] according to the expression

$$\rho_r(T) = \frac{\pi^2}{30} g_\star(T) \frac{k_B^4 T^4}{c^5 \hbar^3}, \quad (2.10)$$

where  $g_\star(T)$  is the effective number of relativistic degrees of freedom,  $k_B$  is Boltzmann's constant, and  $T$  is the temperature. Thus the effective radiation mass density evolves with redshift as  $\rho_r \propto g_\star(1+z)^4$ .

A list of the important particle mass and energy thresholds is given in Table 2.1. Shown in Fig. 2.1 is the corresponding plot of  $g_\star$  as a function of temperature. The factor  $g_\star$  increases by up to a factor  $106.75/3.38 \sim 31.6$  at high redshift when all SM particles are

Table 2.1: Standard model elementary particles and other mass thresholds important in the early universe. Listed are the particles that freeze out below each temperature threshold, the mass of each particle or threshold from [30], the effective relativistic degrees of freedom at the temperature corresponding to that mass threshold, and the change in the degrees of freedom as the radiation temperature of the universe crosses the threshold. See also Fig. 2.1.

Particle(s)	Mass [MeV]	$g_\star$ <sup>a</sup>	$-\Delta g_\star$
All	$> m_{t,\bar{t}}$	106.75	—
$t, \bar{t}$	$1.73 \times 10^5$	96.25	$\frac{7}{8} \cdot 2 \cdot 2 \cdot 3$
$H^0$	$1.26 \times 10^5$	95.25	1
$Z^0$	$9.12 \times 10^4$	92.25	3
$W^\pm$	$8.04 \times 10^4$	86.25	$2 \cdot 3$
$b, \bar{b}$	$4.18 \times 10^3$	75.75	$\frac{7}{8} \cdot 2 \cdot 2 \cdot 3$
$\tau^\pm$	$1.78 \times 10^3$	72.25	$\frac{7}{8} \cdot 2 \cdot 2$
$c, \bar{c}$	$1.28 \times 10^3$	61.75	$\frac{7}{8} \cdot 2 \cdot 2 \cdot 3$
$\Lambda_{\text{QCD}}$ <sup>b</sup>	170	17.25	44.5
$\pi^\pm$	140	15.25	$2 \cdot 1$
$\pi^0$	135	14.25	$1 \cdot 1$
$\mu^\pm$	106	10.75	$\frac{7}{8} \cdot 2 \cdot 2$
$\nu_{\text{dec}}$ <sup>c</sup>	2.6	7.25	$\frac{7}{8} \cdot 2 \cdot 2$
$e^\pm$	0.511	3.38 <sup>d</sup>	$-\Delta g_{\star,f}$ <sup>e</sup>

<sup>a</sup>  $g_\star$  at or below corresponding mass threshold

<sup>b</sup> QCD phase transition [31]; remaining quarks ( $s\bar{s}, d\bar{d}, u\bar{u}$ ) and gluons are bound in hadrons

<sup>c</sup> Neutrino decoupling energy threshold

<sup>d</sup>  $g_\star(T < m_e) = 2 + \frac{7}{8} \cdot 2 \cdot N_{\text{eff}} \cdot (4/11)^{4/3} \sim 3.38$ ; where  $N_{\text{eff}} \sim 3.04$  [25]

<sup>e</sup>  $-\Delta g_{\star,f} = \frac{7}{8} \cdot 2 \cdot 3 - \frac{7}{8} \cdot 2 \cdot N_{\text{eff}} \cdot (4/11)^{4/3}$

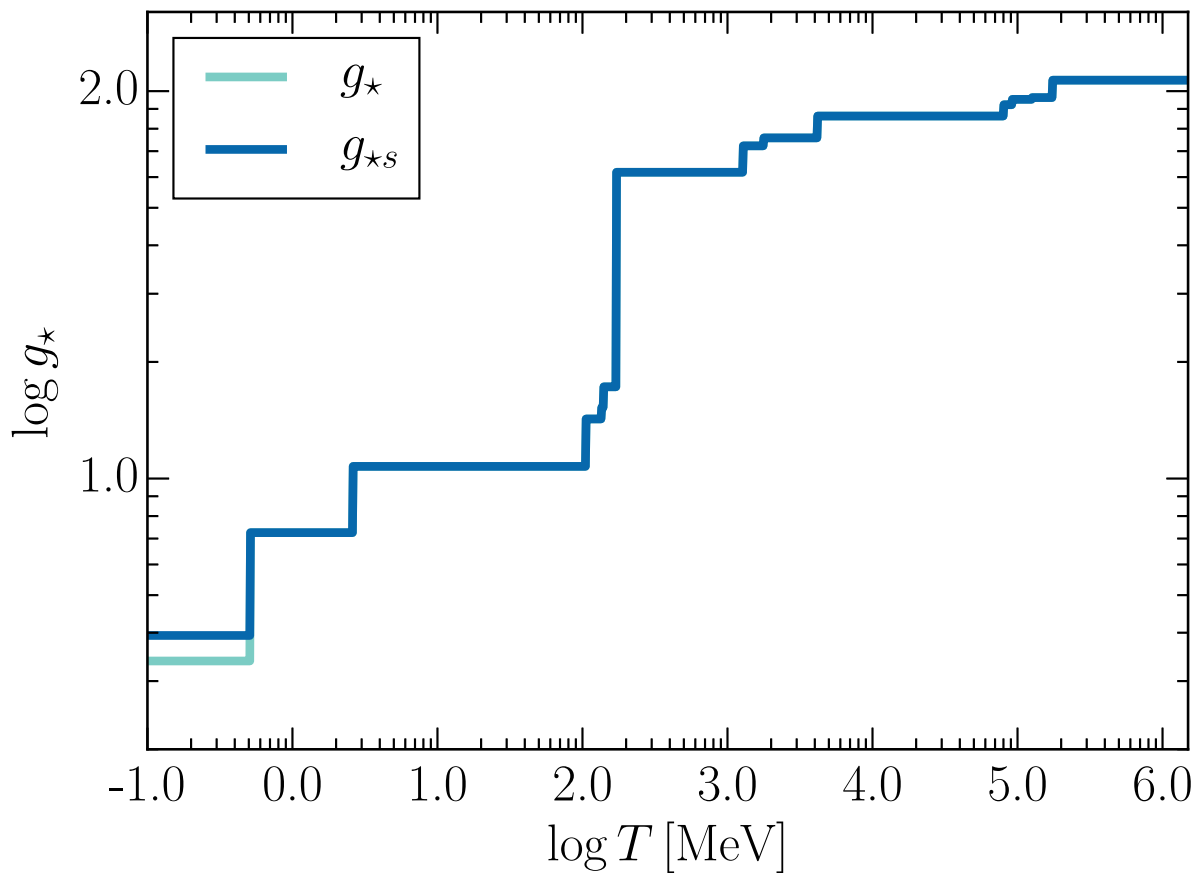


Figure 2.1: Stepwise approximation of  $g_*$  as a function of temperature, including only relativistic particles whose number density is high enough to contribute. Steps occur at temperatures corresponding to the rest mass of elementary SM particles with the largest step occurring at the QCD phase transition scale  $\Lambda_{\text{QCD}} \sim 170$  MeV [31]. The value of  $g_*$  is a minimum for temperatures less than the neutrino decoupling temperature and a maximum for temperatures greater than or equal to the top quark mass. See [28] for a discussion of  $g_{*s}$ .

relativistic. The factor  $g_*(T)$  for all relativistic particle species in thermal equilibrium can be calculated as the sum [28]

$$g_*(T) = \sum_{i=b} g_i \left( \frac{T_i}{T} \right)^4 + \frac{7}{8} \sum_{i=f} g_i \left( \frac{T_i}{T} \right)^4, \quad (2.11)$$

where the first term is the sum over all bosons and the second term is the sum over all fermions.

Each component of the cosmological fluid has an associated temperature whose value depends on redshift. At high redshift after inflation the universe is dominated by radiation and the components of the cosmological fluid are in equilibrium. The temperature of radiation evolves simply as  $T_r = T_0(1+z)$  where  $T_r$  is the radiation temperature at any redshift lower than the neutrino decoupling redshift  $z_{dec,\nu}$  and the temperature today is  $T_0 = 2.72548$  K [32]. The baryonic matter is coupled to the radiation through Compton scattering prior to the thermalization redshift [33]

$$1 + z_{th} \sim 800(\Omega_{b,0}h^2)^{2/5} \sim 174, \quad (2.12)$$

and in this redshift regime the baryonic matter temperature evolves as  $T_b = T_0(1+z)$ . After  $z_{th}$ , the baryonic matter temperature evolves adiabatically until reionization as

$$T_b = T_0 \frac{(1+z)^2}{1+z_{th}}, \quad (2.13)$$

so that at thermalization,  $T_b = T_r(z = z_{th})$ .

It is assumed that the dark matter is mostly weakly interacting massive particles (WIMPs) denoted  $\chi$ . For simplicity other dark matter models are not considered in this study; see [34] for more details on all the dark matter models. For a discussion on the possibility of the PBHs themselves being the dark matter see [13]. If the dark matter is composed of WIMPs the DM temperature decouples from the radiation temperature at high redshift when ther-

mal freeze out of the dark matter particles occurs [34]. The model forces the DM thermal freeze out to occur when  $k_B T_{fr} \sim m_\chi c^2/20$ . If  $m_\chi c^2 = 100$  GeV the freeze out redshift is  $1 + z_{fr} = T_{fr}/T_0 \sim 2 \times 10^{13}$ .

The root-mean-square velocity  $v_{rms}$  is approximated by comparing the relativistic kinetic energy of the dark matter particles to their thermal energy:

$$(\gamma_\chi - 1)m_\chi c^2 = \frac{3}{2}k_B T_\chi, \quad (2.14)$$

where the Lorentz factor associated with  $\beta_\chi \equiv v_{rms}/c$  of the dark matter particles is given by

$$\gamma_\chi \equiv (1 - \beta_\chi^2)^{-1/2}. \quad (2.15)$$

It is useful to define the dimensionless quantity

$$\Theta_\chi \equiv \frac{3k_B T_\chi}{2m_\chi c^2} \quad (2.16)$$

such that Eq. (2.14) becomes  $\gamma_\chi = 1 + \Theta_\chi$  and therefore

$$\beta_\chi^2 = \frac{\Theta_\chi^2 + 2\Theta_\chi}{(1 + \Theta_\chi)^2}, \quad (2.17)$$

which is friendly to numerical evaluations for all possible physical values of  $\Theta_\chi$ . The value of  $\beta_\chi$  becomes close to unity quite rapidly and for the assumed freeze-out temperature,  $\beta_\chi \simeq 0.367$ , i.e. the dark matter particles are mildly relativistic at freeze-out.

## 2.3 Primordial black hole accretion and evaporation

The history of the universe may be divided into redshift regimes to simplify analysis. The relevant physical processes in the very early universe are distinct from those acting in the

current era and thus it is important to summarize the physics in each regime.

Though important to the dynamics of the universe in general, the history of the very early universe (prior to inflation) is not considered in detail in this study. The number density of a pre-inflation cosmological relic, e.g. any pre-inflation PBHs, is negligible after the inflationary epoch. The number density of a pre-inflation relic depends on the amount of inflation. The amount of inflation is calculated by finding the number of  $e$ -foldings during the inflationary epoch

$$N \equiv \int_{a_i}^{a_f} d \ln a = \int_{t_i}^{t_f} H dt, \quad (2.18)$$

where  $t_i$  denotes the start of inflation,  $t_f$  denotes the end of inflation, and  $H$  is the Hubble parameter given in Eq. (2.4). A successful inflation model requires the number of  $e$ -foldings to be at least  $N_{min} \sim 50$  in order to solve the horizon problem [35]. The number density of a relic which formed prior to inflation will thus decrease by a factor  $e^{3N_{min}} \sim e^{150} \sim 10^{65}$ . Thus any PBHs which formed prior to inflation are unlikely to be located in the observable universe today.

After inflation, PBHs may form through a variety of mechanisms including collapse of primordial inhomogeneities, phase transitions, and cosmic string or domain wall collisions [13]. If the energy density fluctuations have a strength  $\delta\rho/\rho \sim 1$  in a particular spacetime volume, the region will likely collapse to a black hole. In this study it is assumed that the collapse to a black hole occurs on a time scale much shorter than the Hubble time so that the expansion is irrelevant to PBH formation. A black hole forming at a time  $t$  after the Big Bang will have a mass less than or equal to the Hubble mass at that time, i.e.

$$M_H = \frac{c^3 t}{G} \sim (4.0 \times 10^{14} \text{ g}) t_{-24}, \quad (2.19)$$

using the useful notation  $f = 10^n f_n$ . At  $t = 1.0$  s after the Big Bang, the Hubble mass is  $M_H \sim 2.0 \times 10^5 M_\odot$ . A derivation of Eq. (2.19) can be found in Appendix A. Models for

the mass function of PBHs are discussed in [13] with emphasis on the behavior of the mass function near the critical mass regime.

Particles with spin  $s$  between energy  $E$  and  $E + dE$  are emitted near the horizon of a Schwarzschild black hole of mass  $M$  at a rate [9, 36]

$$d\dot{N} = \frac{\Gamma_s dE}{2\pi\hbar} \left[ \exp\left(\frac{8\pi GME}{\hbar c^3}\right) - (-1)^{2s} \right]^{-1}, \quad (2.20)$$

where  $\Gamma_s$  is the absorption probability for a mode with spin  $s$  [37]. This is the so-called Hawking radiation which resembles emission from a blackbody with radius  $R_s = 2GM/c^2$  of temperature

$$k_B T_{BH} = \frac{\hbar c^3}{8\pi GM} = (10.6 \text{ MeV}) M_{15}^{-1}. \quad (2.21)$$

The BH can only radiate when the temperature of the hole is greater than that of the radiation bath of the early universe. The temperature of radiation in the early universe evolves as  $T_r \propto 1 + z$  and is less than 10.6 MeV when  $z < 4.5 \times 10^{10}$ , i.e. when  $t > 0.01$  s. This will have a negligible effect on the evolution of PBHs near  $10^{15}$  g. The absorption probability asymptotes to the geometric optics limit

$$\Gamma_s = \frac{27G^2 M^2 E^2}{\hbar^2 c^6} \quad (2.22)$$

when the particle energy is  $E \gg k_B T_{BH}$ . The functional form of  $\Gamma_s$  is much more complicated for lower energy  $E \sim k_B T_{BH}$  interactions as discussed in [37].

The mass loss rate due to the Hawking emission from a Schwarzschild black hole of mass  $M$  requires a sum over all particle types and an integration over the particle energies leading to the simple equation

$$\frac{dM_{15}}{dt} = (-5.34 \times 10^{-5} \text{ g s}^{-1}) f(M) M_{15}^{-2}, \quad (2.23)$$

where  $f(M)$  is a function [36] allowing for the emission of particles other than photons and  $f(M) = 1$  for  $M \gg 10^{17}$  g. The function  $f(M)$  increases when the mass of the PBH crosses a particle mass threshold (see Table 2.1), after which the PBH may emit that particle. A good approximation is  $f(M) \sim f(M_i)$  because for the majority of its lifetime the mass of a PBH remains near its formation mass  $M_i$  [37].

For supermassive black holes or stellar mass black holes the evaporation rate in Eq. (2.23) is negligibly small. The evaporation rate becomes important on cosmological time scales for black holes with mass  $M \sim 10^{15}$  g. This is seen by integrating Eq. (2.23) to get the evaporation timescale

$$t_{evap} = (6.24 \times 10^{18} \text{ s}) f(M_i)^{-1} M_{i,15}^3. \quad (2.24)$$

Assuming  $t_{evap} = t_0 = 13.8$  Gyr, the critical formation mass for evaporation today is

$$M_{cr} = 5.1 \times 10^{14} \text{ g}, \quad (2.25)$$

where the parameter  $f$  for the critical mass is  $f(M_{cr}) \sim 1.9$  as assumed in [13, 36].

In every cosmic era the Hawking evaporation of a near-critical mass PBH will compete with accretion of the cosmological fluid onto the hole. For the PBHs of  $M \sim M_{cr}$  the accretion turns out to be irrelevant if the hole accretes the cosmological fluid at spatially-averaged densities. For PBHs much smaller than  $M_{cr}$  accretion is completely unimportant. For PBHs larger than  $M_{cr}$  the accretion becomes ever more important and the evaporation rate becomes ever smaller. Thus it is important to quantify the various accretion rates at the relevant cosmic epochs. The accretion rates are dependent on the physical parameters of the cosmological fluid, which change dramatically with redshift. The full equation to be solved is the first-order nonlinear ordinary differential equation in  $M$

$$\frac{dM}{dt} = \dot{M}_{evap}(f, M; z) + \dot{M}_{acc}(\rho, c_s, M; z), \quad (2.26)$$

where  $\dot{M}_{evap}$  is given by Eq. (2.23) and the mass accretion term  $\dot{M}_{acc}$  will be calculated in the following sections. The equation is integrated from the formation time  $t_i$  to any desired final time (or the evaporation time for small holes) using Eq. (2.8), with the concordance cosmological model accounted for at all times. The Hawking evaporation term has an explicit dependence on  $f(M)$  and the mass  $M$  of the hole and an implicit dependence on  $z$  (or  $t$ ). The accretion term has explicit dependence on  $\rho$ ,  $c_s$ , and  $M$  and an implicit dependence on  $z$  due to the evolution of those quantities across cosmic time.

The mass accretion term in Eq. (2.26) is split into its component parts

$$\dot{M}_{acc}(\rho, c_s, M; z) = \dot{M}_r + \dot{M}_b + \dot{M}_\chi, \quad (2.27)$$

where  $r$  indicates radiation ( $\gamma$ ,  $\nu$ , and other SM particles),  $b$  indicates baryonic matter, and  $\chi$  the dark matter particles. When the universe is cool enough (i.e.  $T_r < 0.511$  MeV), the radiation term consists only of photons and neutrinos. At higher redshift, the other SM particles become relativistic and can be accreted. When the baryonic matter is coupled to the radiation the two accretion rates become coupled and are written  $\dot{M}_{b+r}$ . In the sections following, the mass accretion term is calculated explicitly for the different cosmic eras.

### 2.3.1 Late universe accretion

In the late universe at  $z \lesssim z_{th}$  the relevant cosmic scales are set by the formation and evolution of structure, i.e. the distribution of dark and baryonic matter in the cosmic web. The details of cosmic structure formation are ripe with rich and complicated physics and are not included in this study; see [38, 39].

To set a bound on late universe accretion, all accretion terms here are set by the spatially-averaged fluid quantities. The PBHs in our universe will likely form and evolve within overdense regions, so the use of spatially-averaged quantities gives a good idea what to expect with relatively isolated holes. The accretion of radiation in this redshift regime is

unimportant for  $\sim M_{cr}$  PBHs because it is a horizon-limited growth given in the approximate form

$$\begin{aligned}
\dot{M}_r &= 4\pi R_S^2 c \rho_r \\
&= \frac{16\pi G^2}{c^3} \rho_{r,0} (1+z)^4 M^2 \\
&= (6.5 \times 10^{-48} \text{ g s}^{-1}) (1+z)^4 M_{15}^2,
\end{aligned} \tag{2.28}$$

where  $\rho_r$  is the equivalent mass density in radiation. The accretion rate in Eq. (2.28) is comparable to the magnitude of the Hawking evaporation rate when the mass of the PBH is

$$M = (6.3 \times 10^{25} \text{ g}) (1+z)^{-1}. \tag{2.29}$$

Thus the accretion of background radiation in this redshift regime is unimportant to critical mass holes. A PBH of the mass given in Eq. (2.29) will not evaporate until long after the current era.

The accretion of baryonic matter is more complicated as it is governed by gas dynamics in the vicinity of the PBH. If the PBH is in an ‘average’ region of the universe, i.e. of average baryonic matter density and temperature, the accretion of baryons will be a competition between Bondi and Eddington-limited accretion [40]. The accretion rate found in this manner will inform a lower bound for any relevant PBH accretion activity. Below  $z \sim 30$  the details of cosmic structure will change this simplified picture, but it is useful to set a first approximation. A complete picture of the baryonic accretion has not been properly solved and is the subject of intense study from both theoretical and observational perspectives. With the complicated gas dynamics removed from the analysis in this simplified calculation,

the accretion rate can be expressed as

$$\begin{aligned}\dot{M}_b &= \min(\dot{M}_{b,B}, \dot{M}_{b,E}) \\ &= \min\left(\frac{4\pi\lambda_s G^2}{c_{s,b}^3} \rho_{b,0}(1+z)^3 M^2, \frac{4\pi G m_p}{\sigma_T c} M\right).\end{aligned}\quad (2.30)$$

where  $\lambda_s = 1/4$  for a  $\gamma = 5/3$  baryonic gas [40],  $m_p$  is the proton mass, and  $\sigma_T$  is the Thomson scattering cross section for electrons. It is clear that the Eddington limit is redshift-independent and is equal to

$$\dot{M}_E = (7.03 \times 10^{-2} \text{ g s}^{-1}) M_{15}.\quad (2.31)$$

The Bondi rate is also redshift-independent in this redshift regime. The temperature of the baryonic gas in this regime is

$$T_b = \frac{T_r(1+z)}{1+z_{th}} = \frac{T_0(1+z)^2}{1+z_{th}},\quad (2.32)$$

and therefore the sound speed in the baryonic gas (assuming it is entirely hydrogen) is

$$\begin{aligned}c_{s,b} &= \left(\frac{5k_B T_b}{3m_p}\right)^{1/2} \\ &= (1+z) \left(\frac{5k_B T_0}{3m_p(1+z_{th})}\right)^{1/2} \\ &= (1.5 \times 10^3 \text{ cm s}^{-1})(1+z).\end{aligned}\quad (2.33)$$

Thus the redshift dependence of the Bondi rate goes away and Eq. (2.30) becomes

$$\begin{aligned}\dot{M}_b &= \min\left[\pi G^2 \left(\frac{5k_B T_0}{3m_p(1+z_{th})}\right)^{-3/2} \rho_{b,0} M^2, \frac{4\pi G m_p}{\sigma_T c} M\right] \\ &= \begin{cases} (1.9 \times 10^{-24} \text{ g s}^{-1}) M_{15}^2, & M < M_{cr,1} \\ (7.0 \times 10^{-2} \text{ g s}^{-1}) M_{15}, & M > M_{cr,1} \end{cases},\end{aligned}\quad (2.34)$$

where  $M_{cr,1} = 3.8 \times 10^{37}$  g is the mass of a PBH that gives an equivalence in the Bondi and Eddington rates in this redshift regime. Comparing Eq. (2.34) to Eq. (2.23) it is clear that an isolated near-critical mass PBH cannot accrete sufficiently to beat the Hawking evaporation rate. The Bondi rate is comparable to the magnitude of the Hawking evaporation rate when the PBH has the characteristic mass

$$M_{ch,1} = 7.3 \times 10^{19} \text{ g.} \quad (2.35)$$

Any relevant growth of a near-critical mass PBH in this redshift regime will have to come from enhanced accretion if the hole is located within a significant density perturbation such as an individual galaxy or galaxy cluster.

### 2.3.2 Post-recombination accretion

In the post-recombination universe ( $z_{th} < z < z_{rec}$ ) the matter temperature is coupled to the radiation temperature via Compton scattering, i.e.  $T_b = T_0(1+z)$ . The recombination redshift is listed in [25] as  $z_{rec} = 1089.90$ . Starting 381,000 yr after the Big Bang and until thermal decoupling, the sound speed in the baryonic gas can be expressed as

$$\begin{aligned} c_{s,b} &= \left( \frac{5k_B T_b}{3m_p} \right)^{1/2} \\ &= (1+z)^{1/2} \left( \frac{5k_B T_0}{3m_p} \right)^{1/2} \\ &= (1.9 \times 10^4 \text{ cm s}^{-1})(1+z)^{1/2}. \end{aligned} \quad (2.36)$$

In this redshift regime, the accretion of radiation is still horizon limited and given by Eq. (2.28). The accretion of baryonic matter is the Bondi accretion rate at lower mass and is

Eddington-limited growth if the mass is large enough. Using the same arguments as before

$$\begin{aligned}
\dot{M}_b &= \min(\dot{M}_{b,B}, \dot{M}_{b,E}) \\
&= \min\left(\frac{\pi G^2}{c_{s,b}^3} \rho_{b,0} (1+z)^3 M^2, \frac{4\pi G m_p}{\sigma_T c} M\right) \\
&= \begin{cases} (8.1 \times 10^{-28} \text{ g s}^{-1})(1+z)^{3/2} M_{15}^2, & M < M_{cr,2} \\ (7.0 \times 10^{-2} \text{ g s}^{-1}) M_{15}, & M > M_{cr,2} \end{cases}, \quad (2.37)
\end{aligned}$$

where  $M_{cr,2} = (8.7 \times 10^{40} \text{ g})(1+z)^{-3/2}$  is the PBH mass that gives an equivalent Bondi and Eddington rate. The Bondi accretion rate in Eq. (2.37) is comparable to the magnitude of the Hawking evaporation rate when the PBH has a characteristic mass

$$M_{ch,2} = (5.1 \times 10^{20} \text{ g})(1+z)^{-3/8}. \quad (2.38)$$

Thus in the post-recombination era until thermal decoupling, the relevant process for near-critical mass PBHs is Hawking evaporation.

### 2.3.3 Pre-recombination accretion

In the pre-recombination era ( $z_{rec} < z < z_{mr}$ ) after matter-radiation equality the baryonic matter and radiation are fully coupled and cannot accrete independently. Thus the assumptions present in the Bondi accretion formula fail [41] and the accretion of the coupled fluid is horizon-limited. The temperature of the baryonic gas is coupled to the radiation temperature and the sound speed in the fluid can be written (see Appendix B)

$$c_s^2 = \frac{c^2}{3} \frac{4\rho_r}{4\rho_r + 3\rho_b}. \quad (2.39)$$

At the matter-radiation equality the sound speed in Eq. (2.39) is a few percent below the asymptotic value  $c/\sqrt{3}$ .

The accretion rate of this coupled fluid onto a PBH is the horizon-limited rate

$$\begin{aligned}
\dot{M}_{b+r} &= 4\pi R_S^2 c_s (\rho_r + \rho_b) \\
&= \frac{16\pi G^2}{\sqrt{3}c^3} \left[ \frac{4\rho_{r,0}(1+z)^4}{4\rho_{r,0}(1+z)^4 + 3\rho_{b,0}(1+z)^3} \right]^{1/2} \\
&\quad \times \left[ \rho_{r,0}(1+z)^4 + \rho_{b,0}(1+z)^3 \right] M^2.
\end{aligned} \tag{2.40}$$

This rate has a complicated dependence on redshift so it is useful to expand the right hand side of Eq. (2.40) near the boundaries of this redshift regime. Defining the intermediary terms  $\rho'_r \equiv 4\rho_{r,0}$  and  $\rho'_b \equiv 3\rho_{b,0}$  near  $z_{rec}$  the rate takes the form

$$\begin{aligned}
\dot{M}_{b+r} &= (6.8 \times 10^{-36} \text{ g s}^{-1}) \left[ 0.26\rho'_r \left( \frac{1+z}{1+z_{rec}} \right)^4 \right. \\
&\quad \left. + 0.17\rho'_b \left( \frac{1+z}{1+z_{rec}} \right)^3 \right] M_{15}^2.
\end{aligned} \tag{2.41}$$

The redshift dependence of the sound speed in Eq. (2.39) is included in the expansion above and in the expansion that follows. The rate in Eq. (2.41) becomes comparable in magnitude to the Hawking evaporation rate when the PBH has a characteristic mass

$$\begin{aligned}
M_{ch,3a} &\simeq (6.2 \times 10^{22} \text{ g}) \left[ 0.26\rho'_r \left( \frac{1+z}{1+z_{rec}} \right)^4 \right. \\
&\quad \left. + 0.17\rho'_b \left( \frac{1+z}{1+z_{rec}} \right)^3 \right]^{-1/4}.
\end{aligned} \tag{2.42}$$

So again the Hawking evaporation is most important for critical mass, i.e. Eq. (2.25), PBHs.

Closer to  $z_{mr}$  the rate in Eq. (2.40) takes the form

$$\begin{aligned}
\dot{M}_{b+r} &= (5.5 \times 10^{-34} \text{ g s}^{-1}) \left[ 0.25\rho'_r \left( \frac{1+z}{1+z_{mr}} \right)^4 \right. \\
&\quad \left. + 0.21\rho'_b \left( \frac{1+z}{1+z_{mr}} \right)^3 \right] M_{15}^2,
\end{aligned} \tag{2.43}$$

so the accretion of the baryonic radiation fluid occurs slowly for near critical PBHs. This rate becomes comparable in magnitude to the Hawking evaporation rate when the hole is of characteristic mass

$$M_{ch,3b} \simeq (2.1 \times 10^{22} \text{ g}) \left[ 0.25 \rho'_r \left( \frac{1+z}{1+z_{mr}} \right)^4 + 0.21 \rho'_b \left( \frac{1+z}{1+z_{mr}} \right)^3 \right]^{-1/4}. \quad (2.44)$$

The accretion of dark matter onto a PBH will be horizon-limited and should be quite small if the spatially-averaged cosmological value for  $\rho_{\chi,0}$  is assumed. The dark matter accretion rate is

$$\dot{M}_\chi = 4\pi R_S^2 c \beta_\chi \rho_\chi, \quad (2.45)$$

where  $\beta_\chi$  is defined in Eq. (2.17). The mass density of dark matter evolves according to  $\rho_\chi = \rho_{\chi,0}(1+z)^3$  such that Eq. (2.45) becomes

$$\dot{M}_\chi = \frac{16\pi G^2}{c^3} \frac{(\Theta_\chi^2 + 2\Theta_\chi)^{1/2}}{1 + \Theta_\chi} \rho_{\chi,0}(1+z)^3 M^2. \quad (2.46)$$

If there is an enhancement of the DM density term  $\rho_\chi$  due to the formation of a DM halo there will be an appropriate enhancement of the DM accretion rate. Thus Eq. (2.46) represents a lower limit on the DM accretion rate. For a treatment of accretion from an enhanced DM halo see [22, 23]. Since the temperature  $T_\chi$  of dark matter decoupled from the radiation temperature at  $z_{fr} \sim 2.1 \times 10^{13}$ , the dimensionless quantity  $\Theta_\chi$  in this redshift regime is quite small. The expansion of  $\beta_\chi$  for  $\Theta_\chi \ll 1$  is  $\beta_\chi \simeq (2\Theta_\chi)^{1/2}$ . Thus Eq. (2.46) becomes

$$\begin{aligned} \dot{M}_\chi &= \frac{16\pi G^2}{c^3} \left[ \frac{3k_B T_0}{m_\chi c^2 (1+z_{fr})} \right]^{1/2} \rho_{\chi,0}(1+z)^4 M^2 \\ &= (3.4 \times 10^{-58} \text{ g s}^{-1})(1+z)^4 M_{15}^2, \end{aligned} \quad (2.47)$$

which is about ten orders of magnitude smaller than the accretion rate due to the baryon-radiation coupled fluid. In this regime the accretion rate of dark matter onto a PBH becomes similar to the Hawking evaporation rate when

$$M_{ch,3c} = (2.3 \times 10^{28} \text{ g})(1+z)^{-1}. \quad (2.48)$$

The constraints on the accretion rates further strengthens the argument that accretion onto a critical mass PBH is unimportant and most if not all of the lifetime of such a PBH is dominated by the Hawking evaporation.

### 2.3.4 Post-DM freeze-out accretion

In the post-DM freeze-out ( $z_{mr} < z < z_{fr}$ ) era the universe is dominated by radiation. The dark matter, if it comprised of WIMPs, will be non-relativistic until redshifts higher than  $z_{fr}$  [34] and will accrete at a horizon-limited rate. The accretion of baryonic matter and radiation is horizon-limited as before. It is convenient to apply  $\rho_b \ll \rho_r$  and therefore ignore the baryonic matter terms and allow  $c_s \sim c/\sqrt{3}$ . Also in this redshift regime, the effective number of relativistic degrees of freedom  $g_\star$  begins to increase at higher redshift so it is important to express the radiation term as in Eq. (2.10). The accretion rate is therefore

$$\begin{aligned} \dot{M}_{b+r} &= 4\pi R_S^2 c_s (\rho_r + \rho_b) \\ &\simeq \frac{8\pi^3 G^2 k_B^4 T_0^4}{15\sqrt{3}c^8 \hbar^3} g_\star (1+z)^4 M^2 \\ &= (2.0 \times 10^7 \text{ g s}^{-1}) \left( \frac{g_\star}{86.25} \right) \left( \frac{1+z}{1+z_{fr}} \right)^4 M_{15}^2. \end{aligned} \quad (2.49)$$

For a near critical mass PBH this is a large accretion rate compared to the magnitude of the Hawking rate. Thus the mass of a PBH in this redshift regime where these two rates

balance is

$$M_{ch,4} = (1.5 \times 10^{12} \text{ g}) \left( \frac{g_\star}{86.25} \right)^{-1/4} \left( \frac{1+z}{1+z_{fr}} \right)^{-1}. \quad (2.50)$$

The period of enhanced accretion in the early universe is quite short due to the strong redshift dependence, i.e.  $\dot{M} \propto (1+z)^4$  so no significant accretion is expected for critical mass PBHs. This is consistent with the findings from previous studies on PBH accretion, i.e. [41]. At high redshift a critical mass PBH will not accrete significantly, but massive PBHs can grow by about an order of magnitude by  $z_{mr}$ .

In this redshift regime the accretion of DM onto the PBH is small. It is increasingly important at higher redshift but is never larger than the radiation accretion rate in Eq. (2.49). At the DM freeze-out redshift the DM particles are somewhat relativistic, i.e.  $\Theta_\chi \sim 0.075$ , such that the accretion rate is of the same form as Eq. (2.47) to a good approximation. In this regime Eq. (2.48) also remains valid.

### 2.3.5 Pre-DM freeze-out accretion

In this redshift regime the universe undergoes many changes as  $g_\star$  increases and all particles become relativistic. At high enough redshifts all particles have the same temperature and follow  $T = T_0(1+z)$ . The accretion rate at these high redshifts is therefore the same as Eq. (2.49). The PBH will not accrete radiation in the early universe if  $T_{BH} > T_r$ , which corresponds to  $z < 4.5 \times 10^{10}$  if  $M = 10^{15}$  g. The radiation accretion at these high redshifts is highly dependent on the particle physics model. This study employs the Standard Model with all the latest particle masses from [30]. The equivalent mass density in radiation changes dramatically in the early universe because of the change in  $g_\star$  as shown in Table 2.1.

Table 2.2 summarizes the relevant properties of the universe with reference to the equations they are first noted. Table 2.3 summarizes the relevant evaporation and accretion rates of PBHs in the relevant redshift regimes with reference to the equations or sections they are

Table 2.2: Properties of the universe across a large range in redshift.

$z$	$\Omega_r$	$\Omega_m$	$\Omega_\Lambda$	$T_r$	$T_b$	$c_s/c$
$z > z_{fr}$	D <sup>a</sup>	N <sup>b</sup>	N	$\propto (1+z)$	$= T_r$	$\sim 3^{-1/2}$
$z_{mr} < z < z_{fr}$	D	N	N	$\propto (1+z)$	$= T_r$	$\sim 3^{-1/2}$
$z_{rec} < z < z_{mr}$	I <sup>c</sup>	D	N	$\propto (1+z)$	$= T_r$	Eq. (2.39)
$z_{th} < z < z_{rec}$	N	D	N	$\propto (1+z)$	$= T_r$	Eq. (2.36)
$z \lesssim z_{th}$	N	D	N	$\propto (1+z)$	Eq. (2.32) <sup>e</sup>	Eq. (2.33) <sup>e</sup>
$z = 0$	N <sup>d</sup>	I <sup>d</sup>	D <sup>d</sup>	$= T_0^d$	Eq. (2.32) <sup>e</sup>	Eq. (2.33) <sup>e</sup>

<sup>a</sup> Dominant component of energy content.

<sup>b</sup> Negligible component of energy content.

<sup>c</sup> Important; non-negligible but non-dominant.

<sup>d</sup>  $\Omega_{r,0} \sim 9 \times 10^{-5}$ ,  $\Omega_{m,0} \sim 0.3089$ ,  $\Omega_{\Lambda,0} \sim 0.6911$ , and  $T_0 = 2.72548$  K; see [25] and [32].

<sup>e</sup> Does not account for reionization around  $z \sim 9$  or effects due to structure formation.

first noted.

## 2.4 Results

From the evaporation and accretion expressions in §2.3 it is possible to construct a rough accretion or evaporation history for any PBH with mass  $M_i$  forming at redshift  $z_i$ . The critical mass holes with  $M_i = M_{cr} \sim 5.1 \times 10^{14}$  g will suffer no significant accretion in their entire lifetime if located in a suitably ‘average’ volume of the universe. They will assume the evaporation timescale in Eq. (2.24) and evaporate according to Fig. 2.2.

If the same PBHs of Fig. 2.2 happened to form later, say at redshift  $z_i = 10^8$ , it would not affect their history due to the small timescales in the early universe. The accretion rate of the cosmological fluid onto larger PBHs at high redshift will be more important.

The analysis in §2.3 can be summarized in a look-up plot of  $M_f$  against  $M_i$ . The regime important for  $M_i \sim 10^{-4} M_\odot$  holes is shown in Fig. 2.3 and the entire mass regime is shown in Fig. 2.4. Note the agreement of Fig. 2.4 in the near-critical mass regime to Figure 2 of

Table 2.3: PBH accretion and evaporation properties across a large range in redshift. This table summarizes the findings of §2.3. In each redshift regime, the accretion rates change due to the changes in  $\rho_i$ ,  $T_r$ ,  $T_b$ , and  $c_s$  as in Table 2.2.

$z$	$\dot{M}_{evap}$ <sup>a</sup>	$\dot{M}_r$	$\dot{M}_b$	$\dot{M}_\chi$ <sup>b</sup>
$z > z_{fr}$	Eq. (2.23)	Eq. (2.49)	—	—
$z_{mr} < z < z_{fr}$	Eq. (2.23)	Eq. (2.49)	Eq. (2.47)	Eq. (2.47)
$z_{rec} < z < z_{mr}$	Eq. (2.23)	Eq. (2.40)	Eq. (2.47)	Eq. (2.47)
$z_{th} < z < z_{rec}$	Eq. (2.23)	Eq. (2.28)	Eq. (2.37)	Eq. (2.47)
$z \lesssim z_{th}$	Eq. (2.23)	Eq. (2.28)	Eq. (2.34)	Eq. (2.47)
$z = 0$	Eq. (2.23)	Eq. (2.28)	Eq. (2.34)	Eq. (2.47)

<sup>a</sup> Since the Hawking evaporation rate  $\dot{M}_{evap} \propto M^{-2}$ , it is only relevant if  $M \lesssim M_{cr}$ . High mass PBHs evaporate long after  $z = 0$ ; see Eq. (2.24)

<sup>b</sup> Does not account for DM halo formation in the late universe due to structure formation. Inside a DM halo the effective mass of the PBH will be enhanced by a potentially large factor  $M \rightarrow f_{halo}M$  and thus  $\dot{M}_\chi \rightarrow f_{halo}^2 \dot{M}_\chi$ .

[21]. The holes evaporating at higher redshift must have initial masses slightly lower than  $M_{cr}$ . Note that no significant accretion occurs across the intermediate mass regime between  $M_{cr}$  and  $\sim 10^{36}$  g due to the low accretion rates for BHs of this mass. Isolated PBHs in this mass regime accreting the spatially-averaged cosmological fluid do not grow much. This does not account for enhancement of the accretion rates due to structure formation and thus represents a first approximation. If the accretion rate is enhanced via  $\dot{M}_{b,B} \rightarrow f_b \dot{M}_{b,B}$  where  $f_b = \rho_{enh}/\rho_b$  is an enhancement factor and  $\rho_{enh}$  is the enhanced baryonic matter density, then a PBH of given initial mass can reach a higher mass for a given final redshift. This is reflected in the dotted lines of Fig. 2.3, which show the final mass of a PBH growing from 1.0 s after the big bang to  $z = 0.1$  given an enhancement factor  $f_b = 10^1, 10^2, 10^3$ . Even a small enhancement of the baryonic matter density leads to a large increase in the possible final mass of the accreting PBH. Since the Bondi accretion rate is proportional to  $M^2$ , higher mass PBHs will accrete more than lower mass PBHs and this increase in the accretion rate is indicated by the increasing  $M_f$  in Fig. 2.3 around  $M \sim 10^{36}$  g.

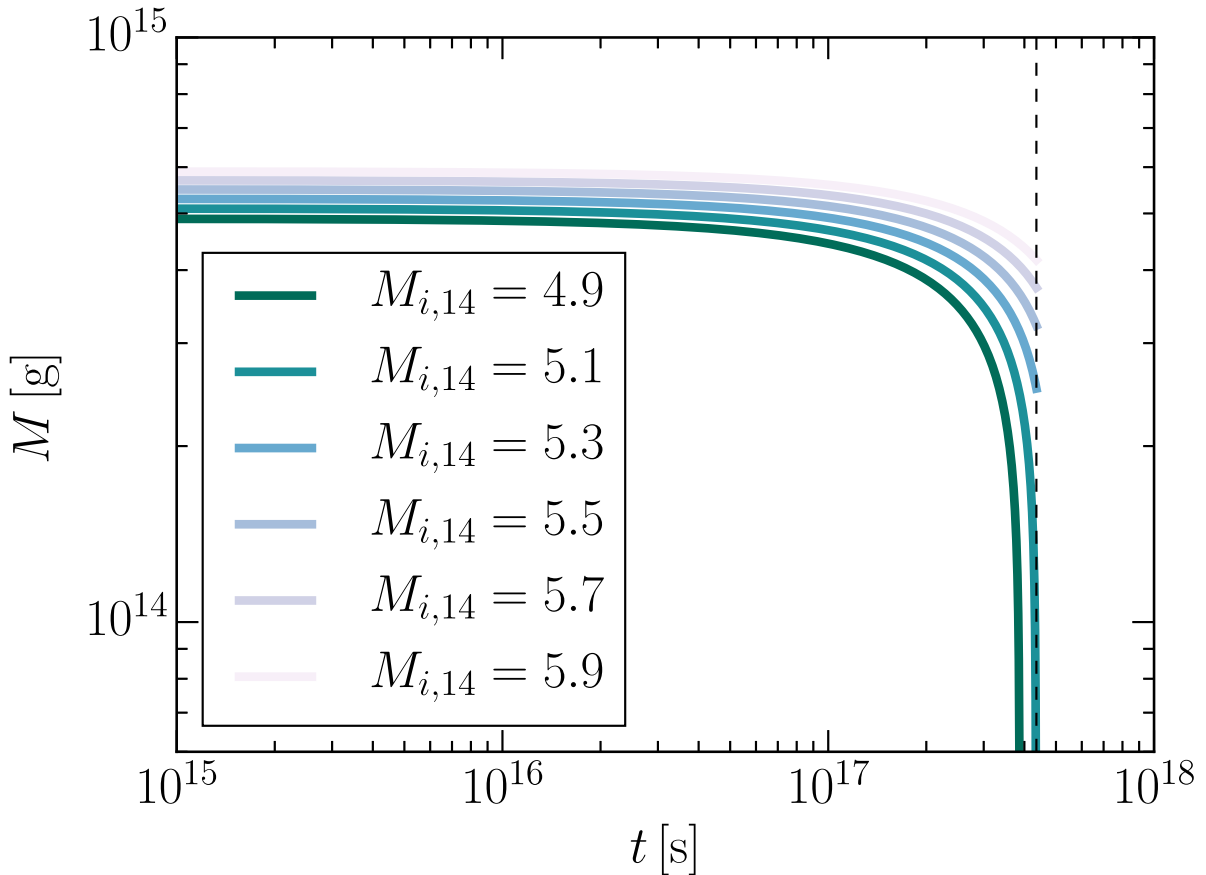


Figure 2.2: Waterfall plot of various PBHs forming at  $z = 10^{16}$  with masses near the critical evaporation mass,  $M_{cr} \sim 5.1 \times 10^{14}$  g. The PBHs near  $M_{cr}$  suffer no significant accretion during their lifetime. The critical mass PBH evaporates at  $t_{evap} = 13.8$  Gyr after the Big Bang (indicated by the dashed line). PBHs with  $M < M_{cr}$  evaporate prior to the current era while those with  $M > M_{cr}$  will evaporate in the future if they do not accrete significantly.

In the first few seconds of the universe ( $z \gtrsim 10^9$ ), PBHs approaching the formation mass limit around  $10^{38}$  g have a large accretion rate (see Eq. 2.49). This large accretion rate, though short-lived, can increase the mass of the PBH by about an order of magnitude by  $z = 10^9$ . This effect is absent in lower mass PBHs and thus is visible in Fig. 2.4 as a small increase beginning above  $M_i \sim 10^{38}$  g.

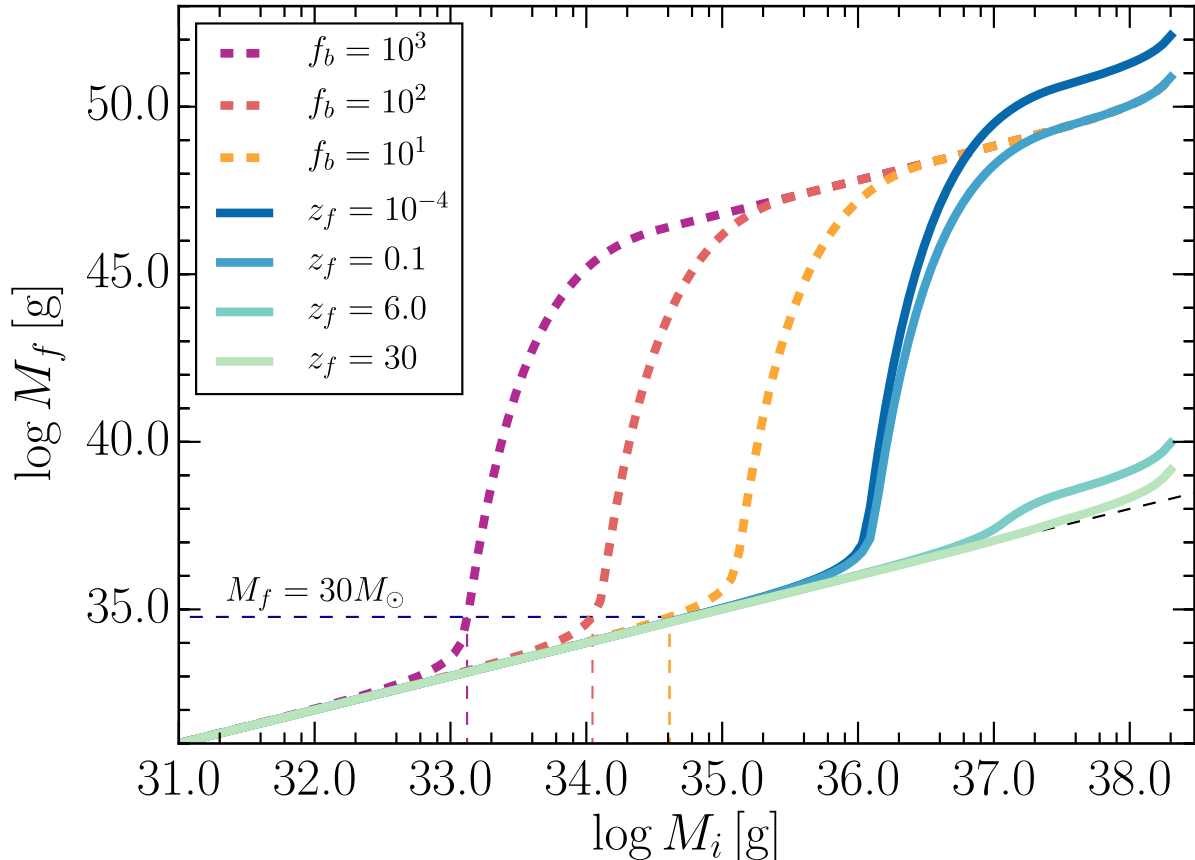


Figure 2.3: Look-up plot of the final mass of PBHs forming at 1.0 s after the Big Bang and ending at redshifts 30, 6, 0.1, and  $10^{-4}$ . Also shown are three cases of PBHs forming at 1.0 s after the Big Bang and ending at  $z = 0.1$  if they are located in a region where  $f_b = 10^1, 10^2$ , and  $10^3$ . The plot shows the dramatic effects of late-universe accretion and density enhancement. It is known from SMBH observations that there are BHs with  $M \sim 2.5 \times 10^{43}$  g at  $z \sim 6.3$  [42]. These holes are not easily explained with our ‘average’ accretion histories; a PBH growing this large would have to be contained in an overdense region of the universe and supplied with gas for their entire histories. Laser Interferometer Gravitational-Wave Observatory (LIGO) observations of the gravitational wave events GW150914 [43] and GW151226 [44] prove the existence of  $\sim 6 \times 10^{34}$  g and  $\sim 3 \times 10^{34}$  g BHs at  $z \sim 0.1$ . These observations are consistent with PBHs inside a regime of higher than average baryonic matter density that grow by a few orders of magnitude over their lifetime. The dotted vertical lines indicate the required initial masses that produce a PBH of  $30M_\odot$  by  $z = 0.1$ . Lower initial masses arise from higher density enhancements  $f_b$ .

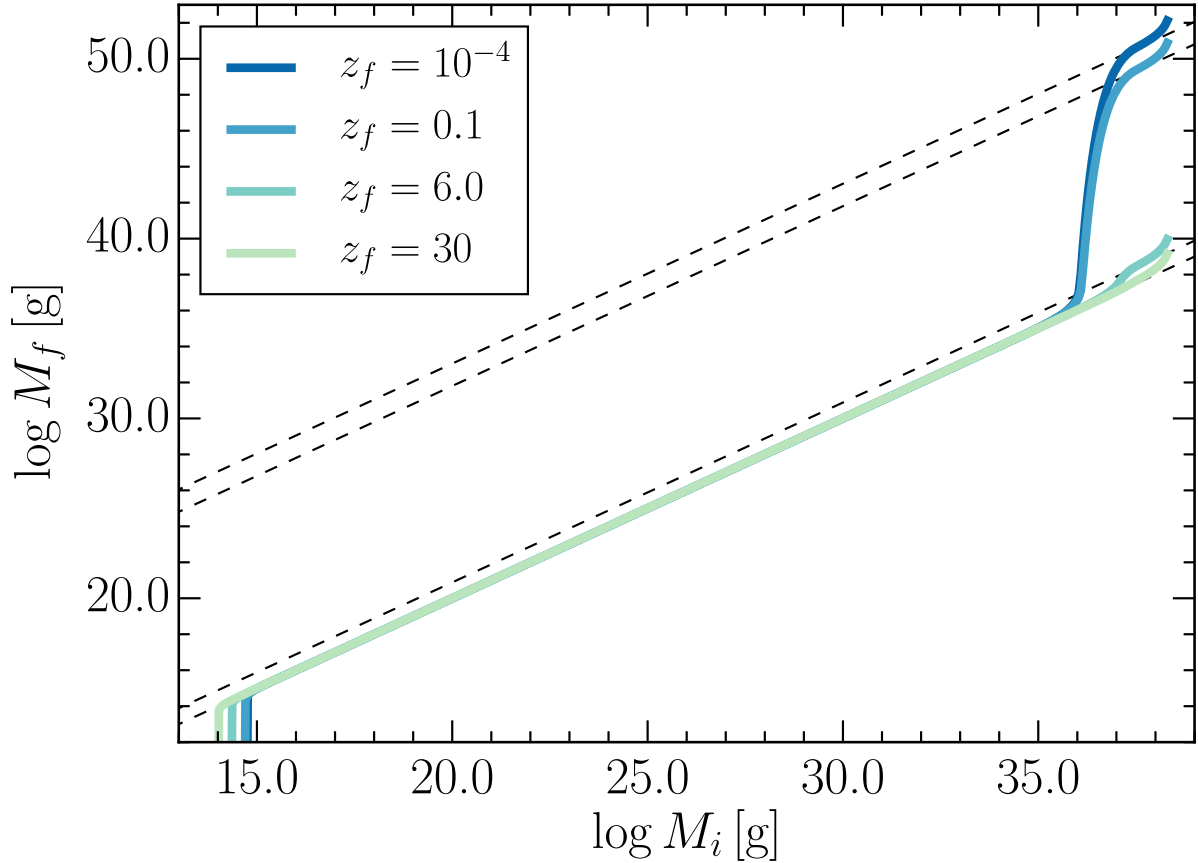


Figure 2.4: Full look-up plot for all PBHs forming at 1.0 s after the Big Bang and ending at redshifts 30, 6, 0.1, and  $10^{-4}$ ; same color scheme as Fig. 2.3. The four dashed lines are  $M_f = 1.1 \times 10^{13} M_i$ ,  $M_f = 6.4 \times 10^{11} M_i$ ,  $M_f = 7.7 M_i$ , and  $M_f = M_i$  (top to bottom). The  $z_f = 30$  case asymptotes to  $M_f = 1.01 M_i$  for  $M_i > 10^{35}$  g. The low-mass regime agrees with Figure 2 of [21], with the cut-off minimum mass increasing for lower final redshift (lower mass PBHs would have already evaporated). The increase in  $M_f$  for  $M_i \sim 10^{38}$  g is due to the large accretion rate of Eq. (2.49) at high redshift, which is large for only a short time due to the  $(1+z)^4$  redshift dependence.

## 2.5 Conclusions and Discussion

A comprehensive view of the evolution of PBHs throughout cosmic history was presented. The accretion and evaporation histories of PBHs with masses in the approximate range  $10^{14} \text{ g} < M < 2 \times 10^{38} \text{ g}$  were calculated. PBHs with lower masses will have evaporated prior to the current era and are not considered and PBHs with higher masses are not allowed due to the Hubble mass constraint of Eq. (2.19). The accreted fluids were assumed to have spatially averaged cosmological densities and the details of structure formation were not included. The important quantities for accretion are the mass densities of the various cosmological fluids, the sound speed in those fluids, and the details of their behavior at all relevant redshifts. All of these details were calculated precisely for the  $\Lambda$ CDM concordance cosmology.

The important findings of this study are the following:

- A PBH with initial mass near  $M_{cr} = 5.1 \times 10^{14} \text{ g}$  will not accrete radiation or matter in any significant quantity and will thus evaporate according to the timescale given in Eq. (2.24). A PBH with initial mass less than  $M_{cr}$  will evaporate prior to the current era.
- A PBH with initial mass in the approximate range  $10^{15} \text{ g} < M_i < 10^{35} \text{ g}$  neither evaporates nor accretes significantly over a Hubble time. Such a PBH would have to grow by other means, i.e. merging with other BHs or accreting while in an overdense region of the universe. Since the Hawking evaporation rate is so small for PBHs in this mass regime, the lower limit on the final (observed) mass of such PBHs is thus simply  $M_f = M_i$ .
- A PBH with initial mass  $M < 10^{38} \text{ g}$  will not grow significantly in the early universe, i.e. within the first few minutes after the Big Bang. This finding is consistent with other PBH accretion studies, e.g. [41]. The small increase for BHs with  $M_i \sim 10^{38} \text{ g}$  seen in Fig. 2.4 results from the large accretion rate for high-mass holes in Eq. (2.49).

It represents a growth of approximately one order of magnitude in the early universe, consistent with previous studies. There is negligible growth of critical mass PBHs in the radiation-dominated era.

- A PBH with initial mass in the approximate range  $10^{35} \text{ g} < M_i < 10^{37} \text{ g}$  can accrete significantly during its lifetime. In the redshift regime  $z_{th} < z < z_{rec}$ , a PBH with  $M < (8.7 \times 10^{40} \text{ g})(1+z)^{-3/2}$  accretes at the Bondi rate and is Eddington-limited above that. In the redshift regime  $z \leq z_{th}$ , a PBH with  $M < 3.8 \times 10^{37} \text{ g}$  accretes at the Bondi rate and is Eddington-limited above that. A PBH with such a mass that grows at the Bondi rate for its whole lifetime can thus grow by one or two orders of magnitude.
- When a PBH grows enough to have its baryonic matter accrete at an Eddington-limited rate, the hole can increase in mass by many orders of magnitude if evolving into the late universe  $z_f \sim 0$ . Since the PBH will grow by accreting the spatially averaged cosmological gas, this growth represents how an ‘average’ PBH accretes at the Eddington limit. The true accretion history of course will be complicated by feedback effects which were not modeled here. The curves in Fig. 2.4 thus represent an ‘average’ growth. A true astrophysical hole of this mass may grow at either a higher or a lower rate.
- A PBH with initial mass in the approximate range  $4 \times 10^{37} \text{ g} < M_i < 10^{38} \text{ g}$  will accrete at an Eddington limited rate after  $z_{rec}$  and the final mass of such a hole depends on its observed redshift. At  $z_f = 30$ , the hole can only grow to  $M_f = 1.01M_i$ . The hole can grow to  $M_f = 7.7M_i$  if  $z_f = 6$ . The hole can grow to  $M_f = 6.4 \times 10^{11}M_i$  if  $z_f = 0.1$  and to  $M_f = 1.1 \times 10^{13}M_i$  if  $z_f = 10^{-4}$ . See Fig. 2.4 for more details.

The PBH mass histories discussed in this study represent a first approximation of their cosmic behavior. Several astrophysical applications may be discussed in the context of the above results:

- It is impossible to explain the large BHs with  $M \sim 10^{10} M_{\odot}$  observed [42] at  $z > 6$  via PBHs with Eddington-limited accretion of the ‘average’ baryonic gas, even with  $M_i \sim 10^5 M_{\odot}$ . These holes must be explained through multiple massive PBH mergers, mergers with BH seeds from the first generation of stars, or PBHs in overdense regions accreting at super-Eddington rates.
- PBHs do not easily grow to  $30M_{\odot}$  by  $z \sim 0.1$  through Bondi accretion of the ‘average’ cosmological fluid. These PBHs cannot easily explain the binary BH mergers observed by LIGO as the gravitational wave events GW150914 [43] and GW151226 [44] unless they experience an enhancement of the Bondi rate through various channels. One such channel is a baryonic matter density enhancement leading to  $\dot{M}_{b,B} \rightarrow f_b \dot{M}_{b,B}$  as discussed in §4. Small enhancement factors allow a lower mass PBH to reach  $30M_{\odot}$  compared to those PBHs accreting the average cosmological baryonic matter. Another possibility is the LIGO BHs were PBHs that formed with an initial mass  $M_i = M_f$ , where  $M_f$  is their mass at the merger time. According to [45], the event rate for PBH mergers would be high enough to explain the GW events if the PBHs constitute a large enough fraction of the dark matter. However, PBHs in the appropriate mass range to explain these LIGO events are unlikely to be a large enough fraction of the DM as constrained from CMB measurements discussed in [46], [47], and [48]. Either LIGO has chanced upon two relatively rare PBH mergers or there is a common stellar evolution channel that produces BHs of these masses. Both explanations are interesting and more data are needed to distinguish these two possibilities.
- Searches for PBH bursts [24] are ongoing. Although there are candidates for such events, no confirmed PBH burst event has been detected. The spectral properties of such bursts should be distinguishable from the ‘normal’ GRBs. The non-detection of such an event has a few explanations. First, the fraction of PBHs that make up the dark matter must be quite low for PBHs of the relevant mass scale (see Fig. 9 of [13]).

Thus it is plausible that not enough of these PBHs exist to subsequently evaporate and trigger gamma-ray detectors. Second, it might be possible for the critical mass holes to accrete enough to no longer evaporate in the current era. However, the accretion rate is too small and this would not explain the non-detection of PBH bursts. Even if the accretion rate onto small PBHs happened to be large enough, there would be smaller PBHs that would accrete enough to reach  $M_{cr}$  anyway, filling the void of critical mass holes.

## Chapter 3

# Transient electromagnetic signature of SMBHB mergers

Black hole binary systems evolve toward irreversible states beginning with a shrinking orbit from accretion disk interactions and ending in gravitational wave emission driving the system to a dramatic merger [49]. A binary supermassive black hole binary (SMBHB) system located deep in a galactic potential well is immersed in the approximately uniform magnetic field created by the inner accretion disk surrounding the SMBHB system. A black hole binary inspiralling within this magnetic field will produce copious isotropic and collimated electromagnetic energy losses that increase in frequency and amplitude until the merger time. A binary black hole merger should not create messy baryon-rich ejecta as in kilonovae, merger events requiring the presence of at least one neutron star [50], rather it will drive a Poynting flux dominated outflow. A SMBHB system with total mass  $10^8 M_\odot$  will produce an isotropic electromagnetic luminosity of  $\simeq 10^{45}$  erg/s that to first post-Newtonian (PN) order scales with the gravitational wave luminosity  $\mathcal{L}_{EM} \lesssim 10^{-11} \mathcal{L}_{GW}$  [51, 52, 53, 54]. The Poynting flux will drive a relativistic blast wave as it interacts with the surrounding interstellar medium (ISM). The synchrotron radiation from this blast wave will radiate across a broad range of EM frequencies and its unique signature will distinguish it from other EM signatures from

the galactic core. This blast wave afterglow will evolve in a similar manner to standard gamma-ray burst afterglow emissions and is the topic of the §3.3.

## 3.1 Special relativity

Wave solutions to the field equations of general relativity emerge from perturbing the Minkowski metric with a small tensor field  $h_{\mu\nu}$ . Astrophysically relevant sources of these gravitational waves include, but are not limited to, compact object mergers, supernovae, and a stochastic background that includes primordial waves from the birth of the universe. The most luminous events in the universe are gravitational waves from compact object mergers. From dimensional analysis their luminosity is scaled by  $\mathcal{L}_{GW} \sim c^5/G \sim 3.6 \times 10^{59}$  erg/s, equivalent to radiating the mass-energy equivalent of  $\sim 2 \times 10^5 M_\odot$  per second.

The discovery of the laws of general relativity by Albert Einstein is an outstanding example of transcendent human intellectual exploration. To understand the importance of this discovery, a discussion on special relativity is in order. Einstein discovered special relativity and the mutability of space and time by taking two simple postulates to their logical termination [55]:

1. **Principle of Relativity:** The laws of electrodynamics are valid for all global Lorentz transformations.
2. **Light celerity invariance:** The celerity of light in empty space,  $c$ , is independent of the motion of the emitting or receiving body.

The postulates of special relativity require a willful recalculation of the basic human experiences of space and time, which are not separate and form a complete spacetime continuum within this framework. A difficult notion to forget is the concept of universal simultaneity, that all observers will agree that some event  $A$  precedes another event  $B$ , a perception explicit in Newtonian (prerelativity) dynamics. Imagine one reference frame  $S$  with coordinate

representation  $(t, x, y, z)$  and another  $S'$  with coordinates  $(t', x', y', z')$  moving at a constant speed  $v = dx/dt$  along the  $x$ -axis without loss of generality. The frames  $S$  and  $S'$  are coincident at  $t = t' = 0$ . The Galilei transformation defines the conversion of the coordinates of events in  $S$  and  $S'$

$$t' = t \quad x' = x - vt \quad y' = y \quad z' = z, \quad (3.1)$$

thus  $t'_A = t_A$  and  $t'_B = t_B$ . Events  $A$  and  $B$  are simultaneous in frame  $S$  if  $t_A = t_B$ . The Galilei transformation then demands simultaneity in frame  $S'$ , namely  $t'_A = t'_B$ , in accordance with everyday experience.

The failure of the Galilei transformation in describing electrodynamical phenomena led Einstein to develop special relativity, in which events in the two inertial reference frames  $S$  and  $S'$  are related by the Lorentz transformation [55]

$$t' = \gamma(t - \beta x/c) \quad x' = \gamma(x - vt) \quad y' = y \quad z' = z, \quad (3.2)$$

where the Lorentz factor  $\gamma \equiv (1 - \beta^2)^{-1/2}$ ,  $\beta \equiv v/c$ , and  $c$  the celerity of light. Event  $A$  is simultaneous to event  $B$  in frame  $S$  if  $t_B - t_A = 0$ . If  $A$  and  $B$  are simultaneous in  $S$  then they cannot be simultaneous in  $S'$  because  $t'_B - t'_A = -(\gamma\beta/c)(x_B - x_A) \neq 0$ . The notion of universal simultaneity is absent in special (and general) relativity.

Hermann Minkowski discovered that special relativity is inherently geometric in nature and introduced the concept of the differential spacetime interval  $ds$  defined via [56]

$$ds^2 \equiv -c^2 dt^2 + dx^2 + dy^2 + dz^2, \quad (3.3)$$

where  $c$  is the speed of light. Events in spacetime are thus separated according to the relative magnitude of the above terms, in other words

$$ds^2 < 0 \quad \text{timelike separated} \quad (3.4)$$

$$ds^2 = 0 \quad \text{lightlike (null) separated} \quad (3.5)$$

$$ds^2 > 0 \quad \text{spacelike separated.} \quad (3.6)$$

Massive observers travel along a timelike trajectory in spacetime (worldline) with a speed  $v < c$ , whereas massless particles (photons, gravitons, etc.) in vacuum travel on null worldlines. An observer cannot travel between two spacelike separated events; doing so would require breaking Postulate 2 above. Though universal simultaneity is absent the causal structure of timelike and null separated events is always preserved, i.e. simultaneity is not preserved only for spacelike separated events.

## 3.2 General relativity and gravitational waves

Though subject to an interesting debate regarding their existence in the first half of the twentieth century, the undeniable reality of wave solutions to the field equations of general relativity appeared in spectacular punctuality one hundred years after their prediction [15]. Gravitational waves propagate at the speed of light, carrying information about the momentum-energy content and geometry of the source system. The information, encoded in the two polarized oscillating GW amplitudes  $h_+(t)$  and  $h_\times(t)$ , falls as  $1/d_L$  where  $d_L$  is the luminosity distance to the source. Extracting GW solutions to the field equations of GR is straightforward and proceeds as follows.

A conceptual realization of the Einstein field equations is written

$$\text{curvature} = \text{stress-energy}, \quad (3.7)$$

or the statement given in [57] “Space acts on matter, telling it how to move. In turn, matter reacts back on space, telling it how to curve.” In mathematical language, the equations are

$$G_{\alpha\beta} \equiv R_{\alpha\beta} - \frac{1}{2}g_{\alpha\beta}R = \frac{8\pi G}{c^4}T_{\alpha\beta}, \quad (3.8)$$

where  $G_{\alpha\beta}$  is the Einstein tensor,  $R_{\alpha\beta} \equiv R^\lambda_{\alpha\lambda\beta}$  is the Ricci curvature tensor (defined as the trace of the Riemann curvature tensor),  $R \equiv R^\lambda_{\lambda}$  is the Ricci scalar (or trace of the Ricci curvature),  $T_{\alpha\beta}$  is the stress-energy tensor,  $G$  is Newton’s gravitation constant (present in order to recover the Newtonian limit), and  $c$  is the speed of light. An excellent review of tensor calculus is found in [58]. The following is a review of the minimum necessary mathematical concepts to understand Eq. (3.8).

The metric tensor, whose components are  $g_{\alpha\beta}$ , is a tensor that defines the dot product in the manifold (our  $D = 3 + 1$  spacetime). The infinitesimal displacement, between two events in the spacetime is invariant and found using the metric tensor

$$ds^2 \equiv g_{\alpha\beta}dx^\alpha dx^\beta. \quad (3.9)$$

In special relativity, the metric tensor is called the Minkowski metric and can be represented as the diagonal matrix

$$g_{\alpha\beta} \equiv \eta_{\alpha\beta} \quad \rightarrow \quad \text{diag}(-1, 1, 1, 1). \quad (3.10)$$

In general relativity one cannot compare a vector to another at a different spacetime location without calculating as well the change in the basis used to find the components. The covariant derivative on a vector  $v$  accomplishes this task and is defined

$$\nabla_\alpha v^\lambda = \partial_\alpha v^\lambda + v^\beta \Gamma^\lambda_{\alpha\beta}, \quad (3.11)$$

where  $\nabla$  is the covariant derivative, the notation  $\partial_\alpha \equiv \partial/\partial x^\alpha$  is used, and the  $\Gamma^\lambda_{\alpha\beta}$  are the connection coefficients defined through

$$\Gamma^\lambda_{\alpha\beta} \equiv \frac{1}{2}g^{\lambda\mu}(\partial_\beta g_{\alpha\mu} + \partial_\alpha g_{\beta\mu} - \partial_\mu g_{\alpha\beta}). \quad (3.12)$$

Since GR is coordinate-independent in the sense that invariant quantities are the same in all coordinate systems, one may be fooled into thinking that a complicated functional form for the components  $g_{\alpha\beta}$  indicates spacetime curvature. This is false; remembering the functional form of basis vectors in a polar coordinate system in Euclidean 3-space removes all doubt. The proper method of assessing spacetime curvature requires knowledge of the change in components of a vector  $w^\alpha$  as it is parallel-transported along a closed path. The process is path-dependent and is given by

$$\delta w^\alpha = R^\alpha_{\beta\mu\nu} w^\beta dx^\mu dx^\nu, \quad (3.13)$$

where  $R^\alpha_{\beta\mu\nu}$  is the Riemann curvature tensor defined as

$$R^\alpha_{\beta\mu\nu} \equiv \partial_\mu \Gamma^\alpha_{\beta\nu} - \partial_\nu \Gamma^\alpha_{\beta\mu} + \Gamma^\alpha_{\lambda\mu} \Gamma^\lambda_{\beta\nu} - \Gamma^\alpha_{\lambda\nu} \Gamma^\lambda_{\beta\mu}. \quad (3.14)$$

All components of the Riemann tensor  $R^\alpha_{\beta\mu\nu} = 0$  in Minkowski spacetime because the space lacks curvature. In general the components are nonzero. The Ricci identity,

$$(\nabla_\mu \nabla_\nu - \nabla_\nu \nabla_\mu) w^\alpha = R^\alpha_{\beta\mu\nu} w^\beta, \quad (3.15)$$

is a statement of the non-commutativity of two covariant derivatives acting on a vector. The fully covariant Riemann curvature tensor has the following symmetries:

$$R_{\sigma\lambda\mu\nu} = -R_{\lambda\sigma\mu\nu} = -R_{\sigma\lambda\nu\mu} = R_{\mu\nu\sigma\lambda}, \quad (3.16)$$

$$R_{\sigma\lambda\mu\nu} + R_{\sigma\nu\lambda\mu} + R_{\sigma\mu\nu\lambda} = 0, \quad (3.17)$$

$$R_{\sigma\lambda\mu\nu} - R_{\mu\nu\sigma\lambda} = 0. \quad (3.18)$$

The Bianchi identity involves covariant derivatives of the Riemann curvature tensor and provides another symmetry

$$\nabla_\lambda R^\alpha{}_{\beta\mu\nu} + \nabla_\nu R^\alpha{}_{\beta\lambda\mu} + \nabla_\mu R^\alpha{}_{\beta\nu\lambda} = 0. \quad (3.19)$$

The Ricci curvature tensor is formed by contracting on the first and third indices of the Riemann curvature tensor

$$\begin{aligned} R_{\alpha\beta} &\equiv g^{\mu\lambda} R_{\mu\alpha\lambda\beta} \\ &= R^\lambda{}_{\alpha\lambda\beta}. \end{aligned} \quad (3.20)$$

The Ricci scalar is the trace of the Ricci curvature tensor

$$\begin{aligned} R &\equiv g^{\mu\lambda} R_{\mu\lambda} \\ &= R^\lambda{}_\lambda. \end{aligned} \quad (3.21)$$

The Bianchi identity of Eq. 3.19 allows the Einstein tensor, defined as

$$G_{\alpha\beta} \equiv R_{\alpha\beta} - \frac{1}{2} g_{\alpha\beta} R, \quad (3.22)$$

to satisfy the contracted Bianchi identity  $\nabla^\beta G_{\alpha\beta} = 0$ .

The stress-energy tensor  $T^{\alpha\beta}$  describes the local energy-momentum density and fluxes. It has zero divergence, i.e.  $\nabla_\beta T^{\alpha\beta} = 0$  and relates to the Einstein tensor via the field equations of Eq. (3.8).

To find a solution to the Einstein field equations is difficult; only a small class of solutions have ever been found. The difficulty arises because in a general sense Eq. (3.8) represents twenty coupled, nonlinear, partial differential equations with each equation having tens to hundreds of terms. Solutions are found by exploiting symmetry and making appropriate approximations.

Wave solutions in general relativity can be found by making the assumption that the spacetime is Minkowskian with a small perturbation

$$g_{\alpha\beta} = \eta_{\alpha\beta} + h_{\alpha\beta}, \quad \text{with } |h_{\alpha\beta}| \ll 1, \quad \text{and} \quad (3.23)$$

$$g^{\alpha\beta} = \eta^{\alpha\beta} - h^{\alpha\beta}, \quad \text{with } |h^{\alpha\beta}| \ll 1. \quad (3.24)$$

In this so-called linearized gravity, the following relationships hold

$$\Gamma^\lambda_{\alpha\beta} = \frac{1}{2}\eta^{\lambda\mu}(\partial_\beta h_{\alpha\mu} + \partial_\alpha h_{\beta\mu} - \partial_\mu h_{\alpha\beta}) + \mathcal{O}(h^2) \quad (3.25)$$

$$R^\alpha_{\beta\mu\nu} = \partial_\mu \Gamma^\alpha_{\beta\nu} - \partial_\nu \Gamma^\alpha_{\beta\mu} + \mathcal{O}(h^2) \quad (3.26)$$

$$R_{\alpha\beta\mu\nu} = \frac{1}{2}(\partial_\mu \partial_\beta h_{\alpha\nu} + \partial_\nu \partial_\alpha h_{\beta\mu} - \partial_\nu \partial_\beta h_{\alpha\mu} - \partial_\mu \partial_\alpha h_{\beta\nu}) + \mathcal{O}(h^2) \quad (3.27)$$

$$R_{\alpha\beta} = \frac{1}{2}(\partial^\lambda \partial_\alpha h_{\beta\lambda} + \partial^\lambda \partial_\beta h_{\alpha\lambda} - \square h_{\alpha\beta} - \partial_\alpha \partial_\beta h) + \mathcal{O}(h^2) \quad (3.28)$$

$$R = \partial^\alpha \partial^\beta h_{\alpha\beta} - \square h + \mathcal{O}(h^2) \quad (3.29)$$

where  $h \equiv \eta^{\sigma\lambda} h_{\sigma\lambda} = h^\lambda_\lambda$  is the trace of the metric perturbation and  $\square \equiv \eta^{\sigma\lambda} \partial_\sigma \partial_\lambda = \partial^\lambda \partial_\lambda$  is the d'Alembertian operator in the background Minkowski spacetime. With the above

relationships, to first order in the perturbing field tensor  $h_{\alpha\beta}$ , Eq. (3.8) becomes

$$\partial^\lambda \partial_\alpha h_{\beta\lambda} + \partial^\lambda \partial_\beta h_{\alpha\lambda} - \square h_{\alpha\beta} - \partial_\alpha \partial_\beta h - \eta_{\alpha\beta} \partial^\lambda \partial^\sigma h_{\lambda\sigma} + \eta_{\alpha\beta} \square h = \frac{16\pi G}{c^4} T_{\alpha\beta}. \quad (3.30)$$

The above equations are difficult to understand on a passing glance. Two choices will simplify the equations. First, introduce the trace-reversed perturbing field tensor

$$\bar{h}_{\alpha\beta} \equiv h_{\alpha\beta} - \frac{1}{2} \eta_{\alpha\beta} h \quad (3.31)$$

such that Eq. (3.30) becomes

$$\partial^\lambda \partial_\alpha \bar{h}_{\beta\lambda} + \partial^\lambda \partial_\beta \bar{h}_{\alpha\lambda} - \square \bar{h}_{\alpha\beta} - \eta_{\alpha\beta} \partial^\lambda \partial^\sigma \bar{h}_{\lambda\sigma} = \frac{16\pi G}{c^4} T_{\alpha\beta}. \quad (3.32)$$

Finally, make a gauge transformation (choice of coordinates) into the harmonic (or Lorenz or de Donder) gauge:  $\partial_\alpha \bar{h}^{\alpha\beta} = 0$ , such that Eq. (3.32) becomes

$$\square \bar{h}_{\alpha\beta} = -\frac{16\pi G}{c^4} T_{\alpha\beta} + \mathcal{O}(h^2). \quad (3.33)$$

One final simplification is to set  $T_{\alpha\beta} = 0$  because the gravitational waves are propagating in empty space. This gives the complete linearized Einstein field equations in the harmonic gauge

$$\square \bar{h}_{\alpha\beta} = 0 + \mathcal{O}(h^2), \quad (3.34)$$

whose solutions are gravitational waves propagating at the speed of light. There is an additional gauge choice that simplifies Eq. (3.34), elucidating the nature of gravitational waves. The convenient choice is to introduce a coordinate transformation

$$x^\lambda \rightarrow x^\lambda + \xi^\lambda \quad \text{with} \quad |\partial_\sigma \xi^\lambda| \ll 1. \quad (3.35)$$

The requirement  $|\partial_\sigma \xi^\lambda| \ll 1$  is a statement that the derivatives of  $\xi^\lambda$  must be small in the same order that the perturbing metric tensor is small, i.e.  $|\bar{h}_{\alpha\beta}| \ll 1$ . In addition, one may demand  $\square \xi_\lambda = 0$  and  $\square(\partial_\sigma \xi_\lambda + \partial_\lambda \xi_\sigma - \eta_{\sigma\lambda} \partial_\mu \xi^\mu) = 0$ . These conditions define the transverse-traceless (TT) gauge. For the perturbing field tensor  $\bar{h}_{\alpha\beta}$ , the traceless condition implies  $\bar{h}^\lambda{}_\lambda \equiv \bar{h} = 0 = h \equiv h^\lambda{}_\lambda$ . The TT gauge removes all time components of the perturbing field tensor such that  $h_{\alpha 0}^{TT} = 0$ . Finally the TT gauge is transverse, namely  $\partial^\beta h_{\alpha\beta} = 0$ .

Solutions to the wave equation  $\square h_{\alpha\beta}^{TT} = 0$  are plane waves

$$h_{\alpha\beta}^{TT} = \mathcal{A}_{\alpha\beta}^{TT} e^{ik_\lambda x^\lambda}, \quad (3.36)$$

where  $k^\lambda \equiv (\omega/c, \mathbf{k})$  is the wave four-vector and  $\mathcal{A}_{\alpha\beta}$  is the amplitude tensor. Without loss of generality, the wave can be taken to be propagating in the  $z$ -direction such that the amplitude tensor is

$$\mathcal{A}_{\alpha\beta}^{TT} = \begin{pmatrix} 0 & 0 & 0 & 0 \\ 0 & h_+ & h_\times & 0 \\ 0 & h_\times & -h_+ & 0 \\ 0 & 0 & 0 & 0 \end{pmatrix}, \quad (3.37)$$

where  $h_+$  and  $h_\times$  are the GW strain amplitudes in the “plus” and “cross” polarization states so named for their effect on a ring of test particles, and the real part of  $e^{ik_\lambda x^\lambda}$  is  $\cos[\omega(t - z/c)]$ .

The stress-energy tensor of the gravitational waves can be found using Eq. (3.8) and evaluating the Einstein tensor to the appropriate order in the perturbing field tensor. In [59] it is shown to be

$$T_{\alpha\beta}^{GW} = \frac{c^4}{8\pi G} \langle \partial_\alpha h_{\mu\nu} \partial_\beta h^{\mu\nu} \rangle, \quad (3.38)$$

where the brackets represent a time average over a few periods of the wave. In the TT gauge, the energy flux of the wave is

$$\begin{aligned}\frac{dE}{dt dA} &= \frac{c^3}{32\pi G} \langle \dot{h}_{ab}^{TT} \dot{h}_{TT}^{ab} \rangle \\ &= \frac{c^3}{32\pi G} \langle \dot{h}_+^2 + \dot{h}_\times^2 \rangle,\end{aligned}\tag{3.39}$$

where, in the first equality, the sum is taken over the time derivatives of the non-zero amplitudes in  $\mathcal{A}_{\alpha\beta}^{TT}$ . The luminosity in gravitational waves is found by integrating the above equations over  $dA = r^2 d\Omega$ , where  $r$  is the distance to the source and  $d\Omega$  is the differential solid angle.

If there is knowledge of the mass distribution of the source of the waves, one may easily calculate the GW energy flux and luminosity. The calculation proceeds as follows. First, assume that the quadrupole moment tensor is the sole source of the GWs (in reality, all moments beyond quadrupole are also needed)

$$I^{ij} = \int d^3x T^{00}(t - r/c, \mathbf{x}) x^i x^j,\tag{3.40}$$

where  $T^{00}/c^2$  is the mass density of the source in the weak field limit. The trace-free quadrupole moment tensor is

$$\mathcal{I}^{ij} = \int d^3x T^{00}(t - r/c, \mathbf{x}) \left( x^i x^j - \frac{1}{3} r^2 \delta^{ij} \right),\tag{3.41}$$

where  $\delta^{ij}$  is the Kronecker delta. The trace-free quadrupole moment tensor projected into the plane orthogonal to the direction of propagation of the GW is the TT quadrupole moment tensor

$$\mathcal{I}_{ij}^{TT} = \left( P_{ik} P_{jl} - \frac{1}{2} P_{ij} P_{kl} \right) \mathcal{I}^{kl},\tag{3.42}$$

where the projection tensor  $P_{ij} \equiv \delta_{ij} - n_i n_j$  and  $n^i \equiv x^i/r$  is the unit normal in the direction of  $x^i$ . With this in mind, the GW energy flux, Eq. (3.39), at a distance  $r$  far from the source can be written

$$\frac{dE}{dt dA} = \frac{G}{8\pi r^2 c^5} \langle \ddot{\mathcal{I}}_{ab}^{TT} \ddot{\mathcal{I}}_{TT}^{ab} \rangle. \quad (3.43)$$

Integrating Eq. (3.43) over  $dA = r^2 d\Omega$  gives the simple result

$$-\frac{dE_{GW}}{dt} = \mathcal{L}_{GW} = \frac{1}{5} \frac{G}{c^5} \langle \ddot{\mathcal{I}}_{ab} \ddot{\mathcal{I}}^{ab} \rangle. \quad (3.44)$$

It can be shown that the GW strain far from the source is then

$$h_{ab}^{TT}(t) = \frac{2G}{c^4 r} \ddot{\mathcal{I}}_{ab}(t - r/c). \quad (3.45)$$

### 3.2.1 GWs from compact binary coalescence

A compact binary coalescence (CBC) is the process wherein two compact objects (either black holes or neutron stars) merge and produce a single compact remnant. The CBC consists of three distinct phases: inspiral, merger, and ringdown. During the inspiral the compact objects (in our case, black holes) emit gravitational radiation, losing energy and angular momentum in the process. The separation between the two BHs adiabatically decreases in a quasi-Keplerian fashion. During the final orbits of the inspiral the Newtonian approximation breaks down, the two BHs plunge toward one another, and the system undergoes a merger, forming a single perturbed BH. The GW luminosity is highest here. The perturbed BH acts similarly to a struck bell, emitting GWs in damped sinusoidal quasi-normal modes (QNMs) that depend on the mass and spin of the remnant BH – the ringdown. It is straightforward to calculate the GW signal during the inspiral. It is also straightforward to calculate the ringdown QNMs. It is impossible, however, to analytically predict the entire CBC gravitational waveform. The inspiral, merger, and ringdown GW signals must be stitched together

numerically to produce the full CBC waveform.

The following mirrors arguments made in [60, 61, 62] regarding the calculation of the quadrupolar GW energy losses. Suppose a black hole binary (BHB) system consists of two Schwarzschild BHs of mass  $m_1$  and  $m_2$  separated by a distance  $r$ , orbiting in the  $xy$ -plane with the  $z$ -axis at an angle  $\iota$  to the line of sight. The total mass is  $m \equiv m_1 + m_2$ , the reduced mass is  $\mu \equiv m_1 m_2 / m$ , the mass ratio is  $q \equiv m_1 / m_2 \leq 1$ , the symmetric mass ratio is  $\eta \equiv \mu / m$ , and the chirp mass is  $\mathcal{M} \equiv \mu^{3/5} m^{2/5}$ . Over the course of a few orbits,  $\dot{r} \simeq 0$  and the orbital angular frequency obeys Kepler's third law, namely  $\Omega^2 r^3 = Gm$ . The nonzero components of the quadrupolar moment tensor are  $\mathcal{I}_{xx}$ ,  $\mathcal{I}_{yy}$ , and  $\mathcal{I}_{xy} = \mathcal{I}_{yx}$ :

$$\mathcal{I}_{xx} = \frac{1}{2} \mu r^2 (1 + \cos 2\varphi), \quad (3.46)$$

$$\mathcal{I}_{yy} = \frac{1}{2} \mu r^2 (1 - \cos 2\varphi), \quad (3.47)$$

$$\mathcal{I}_{xy} = \frac{1}{2} \mu r^2 \sin 2\varphi = \mathcal{I}_{yx}, \quad (3.48)$$

where  $\varphi$  is the orbital phase given by

$$\varphi = \frac{c^3 t}{Gm} \left( \frac{v}{c} \right)^3, \quad (3.49)$$

and  $t$  is the orbital time. The orbital velocity of either mass is  $v$  and it is convenient to write it as the dimensionless parameter

$$\frac{v}{c} = \left( \frac{Gm}{c^3} \pi f \right)^{1/3}, \quad (3.50)$$

where the GW frequency is  $f = 2f_{orb} = \Omega/\pi$  and so the gravitational waves are emitted at twice the orbital frequency. This can be visualized by noting the quadrupolar nature of the GWs and recognizing therefore the requirement of producing two full periods of gravitational waves in one orbital period.

The GW luminosity of such a source can be found using Eq. (3.44) and is written

$$\mathcal{L}_{GW} = \frac{c^5}{G} \mathcal{F}(v), \quad (3.51)$$

where  $\mathcal{F}(v)$  is the flux function and is given by

$$\mathcal{F}(v) = \frac{32}{5} \eta^2 \left( \frac{v}{c} \right)^{10}. \quad (3.52)$$

It is clear in this form that  $\mathcal{L}_{GW}$  increases dramatically toward the final stages of the inspiral when the orbital velocity of the BHs approaches significant fractions of the speed of light.

Making use of Eq. (3.45) and calculating two time derivatives of the quadrupolar moment tensors, the GW strain at a distance  $d_L$  from the source in each polarization state is

$$h_+(t) = \frac{4G}{c^2} \frac{\mu}{d_L} \frac{1 + \cos^2 \iota}{2} \left( \frac{v}{c} \right)^2 \cos 2\varphi \quad (3.53)$$

$$h_\times(t) = \frac{4G}{c^2} \frac{\mu}{d_L} \cos \iota \left( \frac{v}{c} \right)^2 \sin 2\varphi. \quad (3.54)$$

The time derivative of  $v/c$  is simply

$$\frac{d}{dt} \left( \frac{v}{c} \right) = \frac{32}{5} \eta \frac{c^3}{GM} \left( \frac{v}{c} \right)^9, \quad (3.55)$$

and is useful in determining the time to merger given by

$$t_m - t(v) = \frac{5}{256} \frac{1}{\eta} \frac{Gm}{c^3} \left( \frac{v}{c} \right)^{-8}. \quad (3.56)$$

One may also calculate the orbital phase evolution

$$\varphi_m - \varphi(v) = \frac{1}{32} \frac{1}{\eta} \left( \frac{v}{c} \right)^{-5}, \quad (3.57)$$

while recalling  $\varphi_{GW} = 2\varphi$ . Another important quantity is the time derivative of the GW frequency

$$\dot{f} = \frac{96}{5} \left( \frac{GM}{c^3} \right)^{5/3} \pi^{8/3} f^{11/3}. \quad (3.58)$$

The gravitational wave energy released as the orbital velocity increases from  $v_0$  to some  $v$  is given by integrating

$$dE_{GW} = d(v/c) \frac{dt}{d(v/c)} \mathcal{L}_{GW}, \quad (3.59)$$

which gives

$$\begin{aligned} E_{GW}(v) &= \mu c^2 \int_{v_0}^v d(v'/c) \frac{v'}{c} \\ &= \frac{1}{2} \mu c^2 \left[ \left( \frac{v}{c} \right)^2 - \left( \frac{v_0}{c} \right)^2 \right]. \end{aligned} \quad (3.60)$$

Typically  $v_0 \ll v$  if many orbits prior to merger are included in the integration. The energy released in GWs is thus approximately

$$\begin{aligned} E_{GW} &\simeq \frac{1}{2} \mu c^2 \left( \frac{v}{c} \right)^2 \\ &\simeq (8.9 \times 10^{59} \text{ erg}) \mu_8 \left( \frac{v_{-1}}{c} \right)^2, \end{aligned} \quad (3.61)$$

where  $\mu_8$  is the reduced mass in units of  $10^8 M_\odot$  and the orbital velocity  $v_{-1} = 0.1c$ .

The fiducial example of two orbiting supermassive BHs is a non-spinning equal mass BH binary with  $m_1 = m_2 = 10^8 M_\odot$ . The time-domain waveforms are plotted in Fig. 3.1. The characteristic ‘chirp’ signal of the merger showing an increasing frequency is visible in Fig. 3.2. The dimensionless orbital velocity  $v/c$  is shown in Fig. 3.3. The evolution of the gravitational wave phase  $\varphi_{GW}$  is shown in Fig. 3.4.

### 3.2.2 Electromagnetic counterparts of binary black hole mergers

An astrophysical supermassive black hole binary (SMBHB) is likely to be located deep in the potential well of a galaxy and living inside the  $\sim 10^4$  G magnetic field typical of such systems [66]. The SMBHB may initially live inside the interstellar gas at the center of the galaxy, but due to magnetohydrodynamical interactions will decouple from the gas and enter a GW inspiral phase in its evolution.

In their orbital evolution the BHs will move through the magnetic field, tapping the electromagnetic energy present in the field. In simulations, it has been shown that a mainly quadrupolar EM emission is present and follows the phase evolution of the BHs [52, 53, 66, 51]. At quadrupolar order, the EM luminosity is a simple scaling factor  $\sim 10^{-11}$  on the GW luminosity. It is possible to evaluate the evolution of this coincident EM signal through the GW analysis of §3.2.1.

The luminosity of a coincident quadrupolar electromagnetic signal may be expressed as

$$\mathcal{L}_{EM} = \mathcal{F}_{EM} \mathcal{L}_{GW} \quad (3.62)$$

$$= \mathcal{F}_0 \left(\frac{v}{c}\right)^\delta \mathcal{L}_{GW}, \quad (3.63)$$

where  $\delta$  is a power law index on the velocity-dependent term and with the supposition that the constant factor  $\mathcal{F}_0 \sim \mathcal{O}(10^{-11})$ . The EM energy emitted by such a coincident signal is simply

$$E_{EM} = \mu c^2 \mathcal{F}_0 \int_{v_0}^v d(v'/c) \left(\frac{v'}{c}\right)^{1+\delta} \quad (3.64)$$

$$= \mu c^2 \frac{\mathcal{F}_0}{2+\delta} \left[ \left(\frac{v}{c}\right)^{2+\delta} - \left(\frac{v_0}{c}\right)^{2+\delta} \right]. \quad (3.65)$$

A non-singular solution requires  $2 + \delta > 0$  or  $\delta > -2$ . In numerical solutions, these isotropic signals seem to have a small dependence on  $v/c$  such that  $\delta \gtrsim 0$  [53, 66, 51]. The EM energy of this signal is deposited into the interstellar medium via a relativistic blast wave which is

the topic of the next section.

### 3.3 Blastwave afterglow synchrotron emission

A relativistic blastwave compresses the ISM magnetic field and allows electrons present in the outflow to radiate via nonthermal synchrotron emission. The synchrotron emission problem for a population of electrons with a power-law distribution in Lorentz factors is well-posed and has been solved, for example, in [67]. The basic argument is as follows.

The synchrotron emission power,  $dE/dtd\nu$  of a single particle of mass  $m$  and charge  $q$  in a uniform  $B$ -field at pitch angle  $\alpha$  is

$$P(\nu, \gamma) = \frac{\sqrt{3}q^3 B \sin \alpha}{2\pi mc^2} F\left(\frac{\nu}{\nu_{ch}}\right), \quad (3.66)$$

where the characteristic gyration frequency  $\nu_{ch}$  is

$$\nu_{ch} = \frac{3}{4\pi} \gamma^2 \frac{qB \sin \alpha}{mc} \quad (3.67)$$

and

$$F\left(\frac{\nu}{\nu_{ch}}\right) \equiv \left(\frac{\nu}{\nu_{ch}}\right) \int_{\nu/\nu_{ch}}^{\infty} d\xi K_{5/3}(\xi), \quad (3.68)$$

where  $K_{5/3}$  is a modified Bessel function of the second kind [68, 69]. The total synchrotron power of a single electron is the integral of the emission power per unit frequency.

In standard blastwave theory there is a power-law distribution of electron Lorentz factors between a minimum  $\gamma_m$  and a maximum  $\gamma_M$

$$N(\gamma)d\gamma = C_\gamma \gamma^{-p} d\gamma, \quad \text{with } \gamma_m < \gamma < \gamma_M, \quad (3.69)$$

where  $N(\gamma)$  is the number of electrons with Lorentz factor  $\gamma$ ,  $C_\gamma$  is an undetermined constant, and  $p$  is the power law index. The electron population exists in a randomized  $B$ -field such that  $B \sin \alpha \rightarrow \langle B \rangle$ . The averaged  $B$ -field in the comoving (blastwave) frame moving with bulk Lorentz factor  $\Gamma$  with respect to the central engine is denoted  $B'$  and is given by

$$\begin{aligned} B' &= (32\pi m_p \epsilon_B n)^{1/2} \Gamma c \\ &\simeq (0.039 \text{ G}) \epsilon_{B,-2}^{1/2} n_0^{1/2} \Gamma, \end{aligned} \quad (3.70)$$

where  $\epsilon_B$  is the fraction of the blastwave internal energy in the magnetic fields,  $m_p$  is the proton mass,  $n$  is the ambient ISM number density, and the notation for a quantity in cgs units  $Q = 10^n Q_n$  has been used. The minimum electron Lorentz factor is given in [70]:

$$\begin{aligned} \gamma_m &= g(p) \frac{\epsilon_e}{\xi_e} (\Gamma - 1) \frac{m_p}{m_e} \\ &\simeq (1.8 \times 10^2) g(p) \epsilon_{e,-1} (\Gamma - 1), \end{aligned} \quad (3.71)$$

where  $g(p) \simeq \frac{p-2}{p-1}$  for  $p > 2$ ,  $\epsilon_e$  is the fraction of the blastwave internal energy in the shocked electrons,  $m_e$  is the electron mass, and the fraction of shocked electrons that are accelerated is  $\xi_e = 1$ . The observed minimum synchrotron frequency  $\nu_m$  is therefore

$$\begin{aligned} (1+z)\nu_m &= \frac{3}{4\pi} \gamma_m^2 \Gamma \frac{eB'}{m_e c} \\ &\simeq (54 \text{ GHz}) [g(p) \epsilon_{e,-1}]^2 \epsilon_{B,-2}^{1/2} n_0^{1/2} \Gamma^2 (\Gamma - 1)^2. \end{aligned} \quad (3.72)$$

The synchrotron cooling frequency  $\nu_c$  of the population of electrons occurs at a frequency where the electrons lose a significant fraction of their energy to the emission of synchrotron radiation. It is found by comparing the synchrotron emission power to the energy of the

electrons. The electron Lorentz factor associated with this cooling frequency is

$$\begin{aligned}\gamma_c &= \frac{6\pi m_e c}{\sigma_T \Gamma t B'^2 (1 + \tilde{Y})}, \\ &\simeq (5.1 \times 10^6) \epsilon_{B,-2}^{-1} n_0^{-1} t_5^{-1} \Gamma^{-2},\end{aligned}\tag{3.73}$$

where  $\sigma_T \simeq 6.65 \times 10^{-25} \text{ cm}^2$  is the electron Thomson scattering cross section,  $t$  is the time in the observer's frame,  $B'$  is the comoving magnetic field, and  $\tilde{Y}$  are the inverse Compton (IC) corrections, which are taken to be zero in this study. The cooling frequency is thus

$$\begin{aligned}(1+z)\nu_c &= \frac{3}{4\pi} \gamma_c^2 \Gamma \frac{eB'}{m_e c} \\ &\simeq (4.3 \times 10^{18} \text{ Hz}) \epsilon_{B,-2}^{-3/2} n_0^{-3/2} t_5^{-2} \Gamma^{-4}.\end{aligned}\tag{3.74}$$

The last important synchrotron frequency is the frequency at which the radiation is self-absorbed by the same population of electrons. The synchrotron self-absorption (SSA) process occurs when the synchrotron frequency of the radiating electrons matches the synchrotron absorption frequency for the population. The synchrotron photons will be absorbed significantly when the optical depth of absorption is  $\tau_\nu = 1$ , i.e.

$$\tau_\nu = \int_{s_0}^s ds' \alpha_\nu(\nu_a, s') = 1.\tag{3.75}$$

Approximating this integral yields

$$\alpha_\nu \Delta' = 1,\tag{3.76}$$

where  $\Delta' = r/\Gamma$  is the characteristic width of the emission region in the comoving frame. The radius  $r$  of the blast wave is given by the expression

$$r = \frac{\beta c t}{1 - \beta \cos \theta},\tag{3.77}$$

where  $\theta$  is the angle between the line of sight and the emission site. Generally, this method of finding the SSA frequency is difficult to solve. An alternative approach is to estimate the SSA frequency using a blackbody method, equating the specific intensity of a blackbody of temperature  $kT = \gamma m_e c^2$ , with  $\gamma$  the larger of  $\gamma_m$  or  $\gamma_a$ , with the specific intensity of synchrotron radiation at  $\nu_a$ . The cases of different orderings of  $\nu_m$ ,  $\nu_c$ , and  $\nu_a$  will give distinct solutions of  $\nu_a$ .

The specific flux  $F_\nu$  of an electromagnetic signal is related to the specific intensity via

$$I_\nu = \frac{D_A^2}{\pi R_\perp^2} F_\nu, \quad (3.78)$$

where  $D_A$  is the angular diameter distance to the source and  $R_\perp$  is the radius of the spherical shell projected onto the sky and perpendicular to the line of sight. The specific flux can be expressed in terms of the maximum synchrotron power via

$$F_{\nu,max} = (1+z) \frac{N_{tot} P_{\nu,max}}{4\pi D_L^2}, \quad (3.79)$$

where

$$\begin{aligned} P_{\nu,max} &= \Gamma P'_{\nu,max} \\ &= \frac{\sqrt{3}\phi e^3}{m_e c^2} \Gamma B'. \end{aligned} \quad (3.80)$$

Also, assuming all of the swept-up electrons achieve relativistic energies then  $N_{tot} = 4\pi n R_\perp^3/3$ .

The synchrotron spectra will be broken power laws with behavior determined by the ordering of  $\nu_m$ ,  $\nu_a$ ,  $\nu_c$ , and  $\nu_M$ , the comoving magnetic field  $B'(t)$ , and the blastwave dynamics,  $\Gamma(t)$  and  $r(t)$ . This is the standard gamma-ray bust afterglow recipe. Once the dynamics are solved it is a simple manner to calculate the synchrotron spectra and light curves.

There are many starting points one may consider, but as a first step it is simplest to

assume the ad hoc energy conservation  $E_0 = E_{\text{bw}}$ . The blastwave energy can be written

$$\begin{aligned}
E_{\text{bw}} &= \Gamma M c^2 \\
&= \Gamma [M_0 + m + U/c^2] c^2 \\
&= \Gamma [M_0 + m + (\Gamma - 1)m] c^2 \\
&= \Gamma M_0 c^2 + \Gamma^2 m c^2,
\end{aligned} \tag{3.81}$$

where  $M_0$  is the initial blastwave mass,  $m$  is the swept-up ISM mass, and  $\Gamma$  is the bulk Lorentz factor of the blastwave. The initial energy  $E_0$  can be expressed as the sum

$$E_0 = m c^2 + \int_0^T dt' \mathcal{L}_{EM}, \tag{3.82}$$

so that the energy conservation condition gives

$$m c^2 + \int_0^T dt' \mathcal{L}_{EM} = \Gamma M_0 c^2 + \Gamma^2 m c^2. \tag{3.83}$$

This is clearly nonlinear. The goal is to find expressions for  $\Gamma(t)$  and  $m(t)$ . The swept-up mass is simply

$$m = \frac{4\pi}{3} r^3 \rho. \tag{3.84}$$

The radius of the blast wave is  $r \simeq 2\Gamma^2 ct$ . The density can be expressed with an arbitrary power-law dependence on  $r$  via  $\rho = n m_p = n_0 m_p (r/r_0)^{-k}$ , where  $k = 0$  is the constant-density ISM case and  $k = 2$  is a wind medium. Compiling all these relations, the swept-up mass can be expressed as

$$\begin{aligned}
m &= \frac{4\pi}{3} (2\Gamma^2 ct)^3 n_0 m_p \left( \frac{2\Gamma^2 ct}{r_0} \right)^{-k} \\
&= \frac{2^{5-k}}{3} \pi c^{3-k} r_0^k n_0 m_p \Gamma^{6-2k} t^{3-k}.
\end{aligned} \tag{3.85}$$

For the constant density ISM case,

$$m_{\text{ISM}} = \frac{32\pi}{3} c^3 n_0 m_p \Gamma^6 t^3. \quad (3.86)$$

For the wind medium case,

$$m_{\text{wind}} = \frac{8\pi}{3} c r_0^2 n_0 m_p \Gamma^2 t. \quad (3.87)$$

Using these results it is easy to write down the energy conservation condition  $f(\Gamma, t) = E_{\text{bw}} - E_0 = 0$  for each case.

General  $k$

$$f(\Gamma, t) = \frac{2^{5-k}}{3} \pi c^{5-k} r_0^k n_0 m_p \Gamma^{6-2k} (\Gamma^2 - 1) t^{3-k} + \left( \frac{\Gamma}{\Gamma_0} - 1 \right) \int_0^T dt' \mathcal{L}_{EM} = 0. \quad (3.88)$$

Constant density ISM ( $k = 0$ )

$$f(\Gamma, t) = \frac{32\pi}{3} c^5 n_0 m_p \Gamma^6 (\Gamma^2 - 1) t^3 + \left( \frac{\Gamma}{\Gamma_0} - 1 \right) \int_0^T dt' \mathcal{L}_{EM} = 0. \quad (3.89)$$

Wind medium ( $k = 2$ )

$$f(\Gamma, t) = \frac{8\pi}{3} c^3 r_0^2 n_0 m_p \Gamma^2 (\Gamma^2 - 1) t + \left( \frac{\Gamma}{\Gamma_0} - 1 \right) \int_0^T dt' \mathcal{L}_{EM} = 0. \quad (3.90)$$

These are relatively well-behaved for physically plausible values of  $\Gamma$  but since they are highly nonlinear, a root finder is needed to find  $\Gamma(t)$ . A robust algorithm for finding the roots of the general equation  $f(\dots, t) = 0$  is the Van Wijngaarden-Dekker-Brent method, which I will call the VDB method for brevity. The VDB method is useful when the functional form of  $df/dt$  is unknown and relies only on functional evaluations. It combines the methods of root bracketing, bisection, and interpolation and is guaranteed at least linear convergence.

Once one solves for  $\Gamma(t)$ ,  $r(t)$ , and  $B'(t)$ , it is straightforward to calculate the transient and evolving broken power-law synchrotron spectra and light curves. We will publish the results of such a calculation later this year. Though incomplete, this chapter described a new type of transient EM counterpart to SMBHB coalescence events. The signature should be unique and have an interesting evolution in time. The future of astronomy is multi-messenger; a combination of EM and GW signals (perhaps with neutrino signals as well) carries much more information about the system than a single type of signal alone. If the first SMBHB coalescence is discovered through pulsar timing techniques there is a potential for radio telescopes around the world to search for this new type of EM counterpart. If pulsar timing is unsuccessful in discovering GW signals prior to the launch of the Laser Interferometer Space Antenna (LISA), then surely LISA will be. The field of EM counterpart studies is only just beginning!

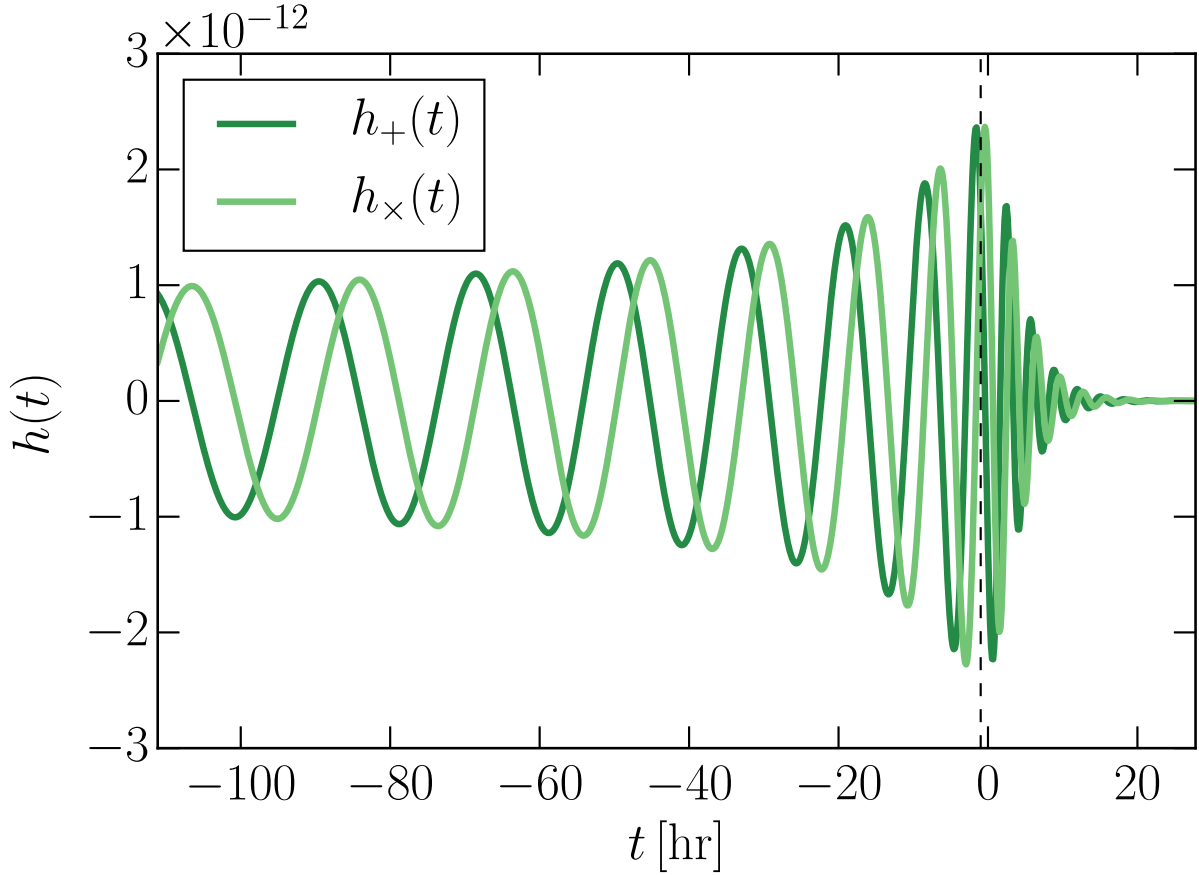


Figure 3.1: Non-spinning equal mass  $10^8 M_\odot$  SMBHB time domain gravitational wave strain. The luminosity distance of the binary is taken to be  $d_L = 1.0$  Mpc and the initial GW frequency is  $f_0 = 0.01$  mHz. The dark and light green curves are the ‘plus’ and ‘cross’ polarization time domain waveforms, respectively. Shown are the final few orbits of the inspiral, the merger, and the ringdown. The vertical black dotted line is the time of maximum GW strain. The waveforms were calculated with PyCBC using the SEOBNRv4 waveform approximant, which stitches together the effective one body inspiral and merger waveforms with the ringdown waveform [63, 64, 65].

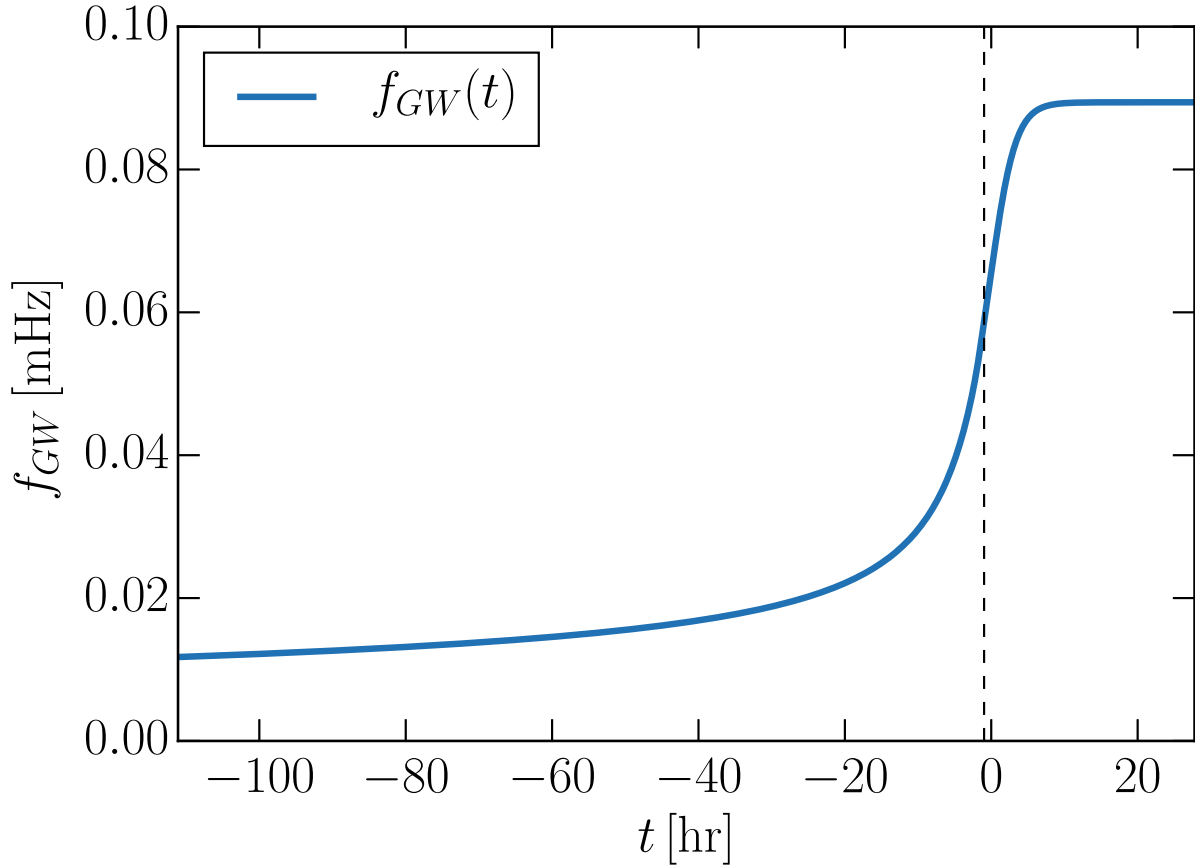


Figure 3.2: Non-spinning equal mass  $10^8 M_\odot$  SMBHB frequency evolution. This is the same system as in Fig. 3.1. The luminosity distance of the binary is taken to be  $d_L = 1.0$  Mpc and the initial GW frequency is  $f_0 = 0.01$  mHz. At the merger time, indicated by the vertical black dotted line, the GW frequency is approximately 0.06 mHz. The frequency evolution was calculated with PyCBC using the SEOBNRv4 waveform approximant [63, 64, 65].

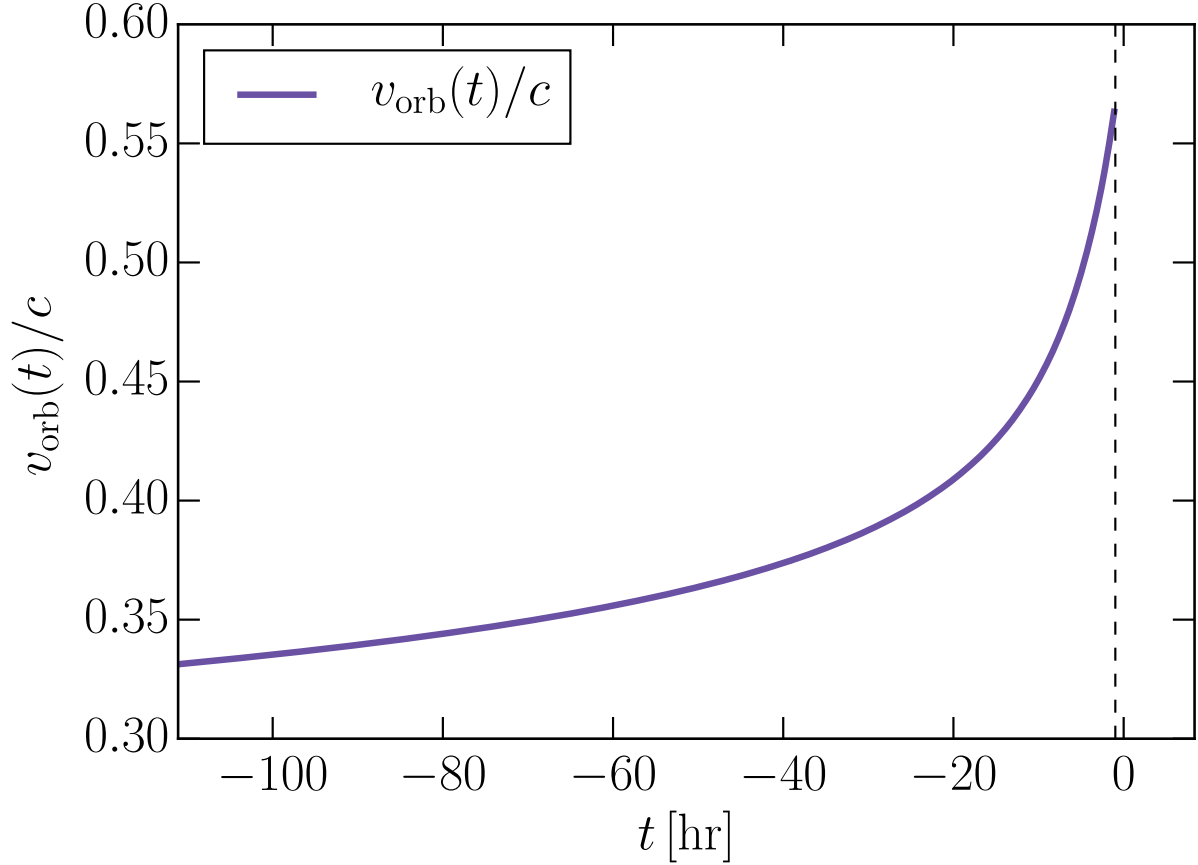


Figure 3.3: Non-spinning equal mass  $10^8 M_{\odot}$  SMBHB dimensionless orbital velocity. This is the same system as in Fig. 3.1. The luminosity distance of the binary is taken to be  $d_L = 1.0$  Mpc and the initial GW frequency is  $f_0 = 0.01$  mHz. At the merger time, indicated by the vertical black dotted line, the dimensionless orbital velocity is approximately  $v/c \sim 0.57c$ . The velocity evolution was calculated with PyCBC using the SEOBNRv4 waveform approximant [63, 64, 65].

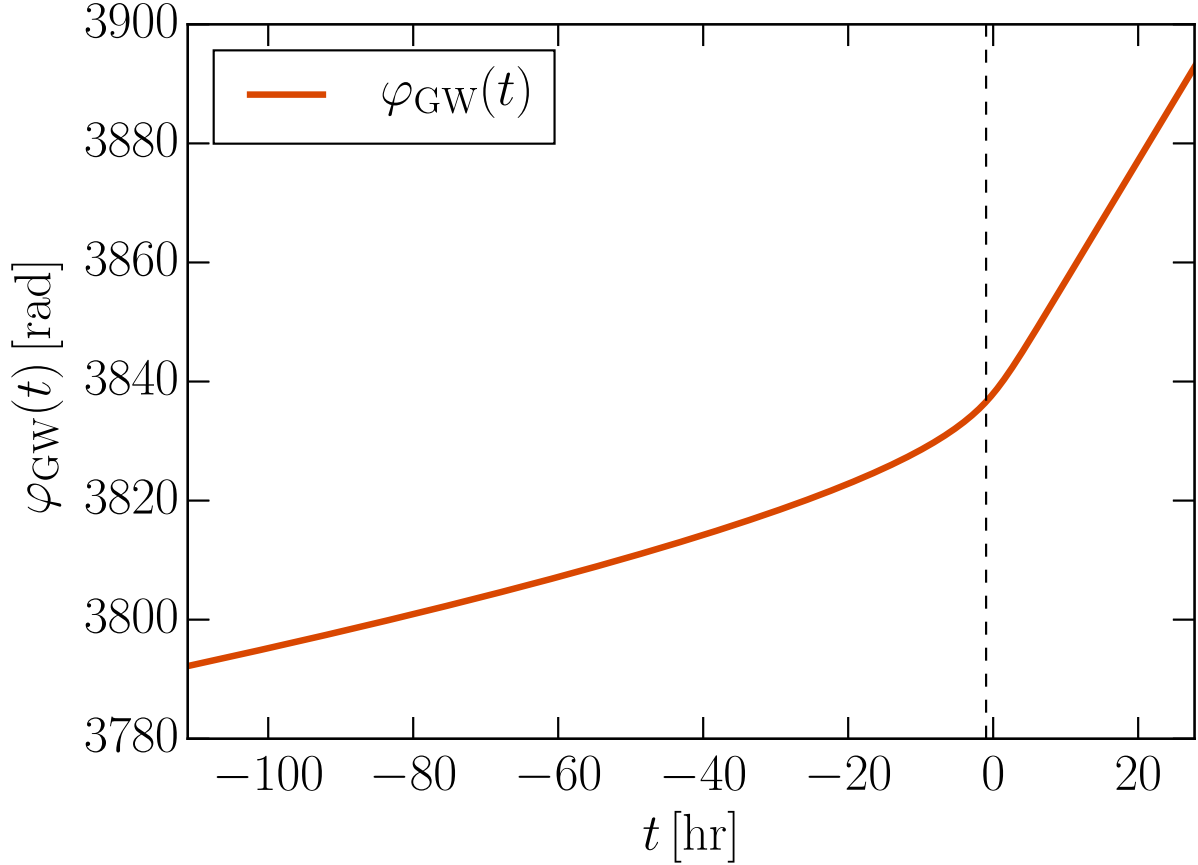


Figure 3.4: Non-spinning equal mass  $10^8 M_\odot$  SMBHB GW phase. This is the same system as in Fig. 3.1. The luminosity distance of the binary is taken to be  $d_L = 1.0$  Mpc and the initial GW frequency is  $f_0 = 0.01$  mHz. The initial gravitational wave phase is 0.0 rad. At the merger time, indicated by the vertical black dotted line, the gravitational wave phase is approximately 3836 rad. The phase evolution was calculated with PyCBC using the SEOBNRv4 waveform approximant [63, 64, 65].

# Appendix A

## Maximum PBH formation mass

As discussed in §2.3 the maximum formation mass of a PBH will be the Hubble mass, i.e. the mass contained within the Hubble volume at a given time. The Hubble radius in the early radiation-dominated universe is  $R_H = 2ct = cH^{-1}$ . Thus the Hubble volume for  $z \gtrsim z_{mr}$  is

$$\begin{aligned} V_H &= \frac{4\pi}{3} R_H^3 \\ &= \frac{32\pi}{3} c^3 t^3, \end{aligned} \tag{A.1}$$

The critical density for the universe to close is the Hubble mass in a Hubble volume and thus the Hubble mass is

$$\begin{aligned} M_H(t) &= \rho_{cr} V_H \\ &= \frac{3H^2}{8\pi G} \cdot \frac{32\pi}{3} c^3 t^3 \\ &= \frac{c^3 t}{G}, \end{aligned} \tag{A.2}$$

which recovers Eq. (2.19). These relations predict only an approximate maximum PBH formation mass, namely that  $M_{PBH} \lesssim M_H$  [13, 21].

# Appendix B

## Sound speed in the cosmological fluid

In the late universe at redshifts lower than  $z_{th}$ , the temperature of the baryonic matter decouples from the CMB photon temperature. Thus the sound speed in the baryonic fluid is given by Eq. (2.33)

$$c_{s,b} = (1.5 \times 10^3 \text{ cm s}^{-1})(1 + z), \quad (\text{B.1})$$

where the increase due to reionization around  $z \sim 9$  is not taken into account. In the redshift regime  $z_{th} < z < z_{rec}$  the redshift dependence changes due to the temperature coupling between the baryonic matter and the CMB radiation. Thus the sound speed evolves as Eq. (2.36)

$$c_{s,b} = (1.9 \times 10^4 \text{ cm s}^{-1})(1 + z)^{1/2}. \quad (\text{B.2})$$

In the above equations it is assumed that the baryonic matter is composed entirely of hydrogen; corrections due to the helium and metal content of the baryonic matter need to be made for a more realistic calculation.

In the early universe at redshifts higher than the recombination redshift  $z_{rec} \sim 1090$ , the baryonic matter is coupled to the CMB radiation. The sound speed in such a coupled fluid

can be found by calculating

$$c_s^2 = \left( \frac{\partial P}{\partial \rho} \right)_s, \quad (\text{B.3})$$

where the subscript  $s$  on the right hand side indicates taking the derivative at constant entropy. The dominant pressure term is the radiation pressure and the density is a sum of radiation and baryonic terms  $\rho = \rho_r + \rho_b$ . The dark matter does not contribute to the pressure or density terms but has an early influence when it is relativistic at redshifts greater than  $z_{fr} \sim 2.1 \times 10^{13}$ .

Rewriting the partial derivatives of Eq. (B.3) in terms of temperature gives

$$c_s^2 = \frac{(\partial P_r / \partial T)_s}{(\partial \rho_r / \partial T)_s + (\partial \rho_b / \partial T)_s}. \quad (\text{B.4})$$

Recalling Eq. (2.10) and  $P_r = \rho_r c^2 / 3$  the numerator of Eq. (B.4) is

$$\left( \frac{\partial P_r}{\partial T} \right)_s = \frac{4\pi^2}{90} g_*(T) \frac{k_B^4 T^3}{c^3 \hbar^3} = \frac{4\rho_r c^2}{3T}, \quad (\text{B.5})$$

ignoring the small  $\partial g_*/\partial T$  terms. Similarly, the first term in the denominator of Eq. (B.4) is

$$\left( \frac{\partial \rho_r}{\partial T} \right)_s = \frac{4\pi^2}{30} g_*(T) \frac{k_B^4 T^3}{c^5 \hbar^3} = \frac{4\rho_r}{T}. \quad (\text{B.6})$$

Recalling at high redshift the radiation and baryonic gas temperatures are coupled, i.e.  $T_r = T_b = T$  and using  $T = T_0(1+z)$ , the second term in the denominator of Eq. (B.4) is

$$\left( \frac{\partial \rho_b}{\partial T} \right)_s = \frac{\partial}{\partial T} \left( \frac{\rho_{b,0} T^3}{T_0^3} \right) = \frac{3\rho_b}{T}. \quad (\text{B.7})$$

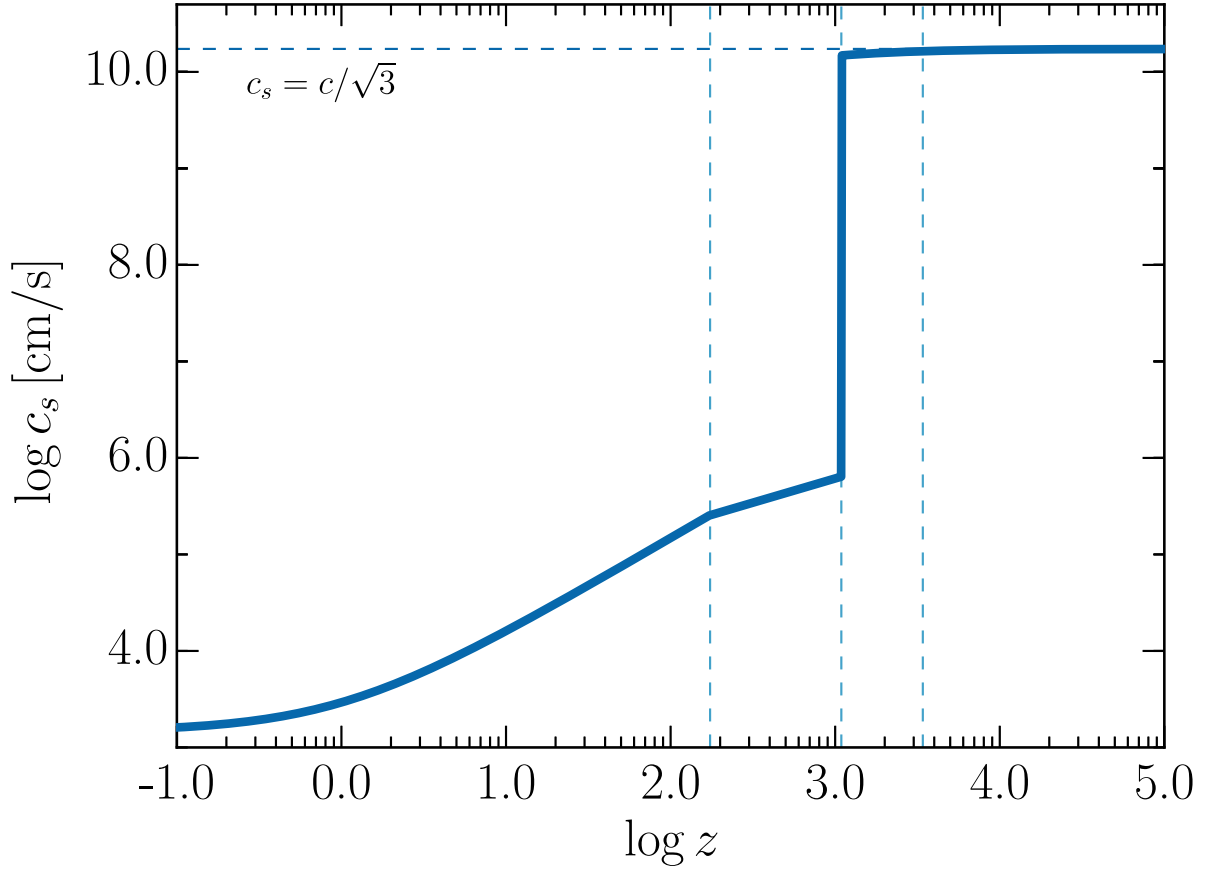


Figure B.1: Plot of sound speed in the baryonic gas against redshift. The sound speed asymptotes to  $c/\sqrt{3} \sim 0.577c$  quickly after the recombination redshift. The three vertical dashed lines are (left to right)  $z_{th}$ ,  $z_{rec}$ , and  $z_{mr}$ . The large jump at  $z_{rec}$  is due to the decoupling of radiation and matter, which reduces the pressure.

Combining Eq. (B.5–B.7) into Eq. (B.4) gives

$$c_s^2 = \frac{c^2}{3} \frac{4\rho_r}{4\rho_r + 3\rho_b}. \quad (\text{B.8})$$

It is clear that at redshifts higher than  $z_{mr} \sim 3400$  the sound speed calculated using Eq. (B.8) asymptotes to  $c_s \sim c/\sqrt{3} \sim 0.577c$ . The behavior of the sound speed across all relevant redshifts is plotted in Fig. B.1.

# Appendix C

## Gravitational wave luminosity

The gravitational wave luminosity of Eq. (3.44) is found by expanding Eq. (3.43) given the definition in Eq. (3.42). The following identities are also useful, given the projection tensor  $\mathcal{P}_{ij} \equiv \delta_{ij} - n_i n_j$  and unit normal  $n^i \equiv x^i/r$ :

$$\mathcal{P}_{ij} = \mathcal{P}_{ji} \tag{C.1}$$

$$n_i n^i = \frac{1}{r^2} x_i x^i = 1 \tag{C.2}$$

$$n^i \mathcal{P}_{ij} = n^i \delta_{ij} - n^i n_i n_j = 0 \tag{C.3}$$

$$\begin{aligned} \mathcal{P}_{ij} \mathcal{P}^{jk} &= (\delta_{ij} - n_i n_j) (\delta^{jk} - n^j n^k) \\ &= \delta_{ij} \delta^{jk} - \delta_{ij} n^j n^k - \delta^{jk} n_i n_j + n_i n_j n^j n^k \\ &= \mathcal{P}_i^k \end{aligned} \tag{C.4}$$

$$\begin{aligned} \mathcal{P}_{ij} \mathcal{P}^{ij} &= (\delta_{ij} - n_i n_j) (\delta^{ij} - n^i n^j) \\ &= \delta_{ij} \delta^{ij} - \delta_{ij} n^i n^j - \delta^{ij} n_i n_j + n_i n_j n^i n^j \\ &= 2 \end{aligned} \tag{C.5}$$

$$\begin{aligned} \mathcal{P}_{ij} \ddot{\mathcal{I}}^{ij} &= \delta_{ij} \ddot{\mathcal{I}}^{ij} - n_i n_j \ddot{\mathcal{I}}^{ij} \\ &= -n_i n_j \ddot{\mathcal{I}}^{ij}. \end{aligned} \tag{C.6}$$

Given these definitions, Eq. (3.43) becomes

$$\begin{aligned}
\frac{dE}{dt dA} &= -\frac{G}{8\pi r^2 c^5} \langle \ddot{\mathcal{I}}_{ab}^{TT} \ddot{\mathcal{I}}_{TT}^{ab} \rangle \\
&= -\frac{G}{8\pi r^2 c^5} \left\langle \left( \mathcal{P}_{ac} \mathcal{P}_{bd} - \frac{1}{2} \mathcal{P}_{ab} \mathcal{P}_{cd} \right) \ddot{\mathcal{I}}^{cd} \left( \mathcal{P}_j^a \mathcal{P}_k^b - \frac{1}{2} \mathcal{P}^{ab} \mathcal{P}_{jk} \right) \ddot{\mathcal{I}}^{jk} \right\rangle \\
&= -\frac{G}{8\pi r^2 c^5} \left\langle \left( \mathcal{P}_{ac} \mathcal{P}_{bd} \mathcal{P}_j^a \mathcal{P}_k^b - \frac{1}{2} \mathcal{P}_{ac} \mathcal{P}_{bd} \mathcal{P}^{ab} \mathcal{P}_{jk} - \frac{1}{2} \mathcal{P}_{ab} \mathcal{P}_{cd} \mathcal{P}_j^a \mathcal{P}_k^b \right. \right. \\
&\quad \left. \left. + \frac{1}{4} \mathcal{P}_{ab} \mathcal{P}_{cd} \mathcal{P}^{ab} \mathcal{P}_{jk} \right) \ddot{\mathcal{I}}^{cd} \ddot{\mathcal{I}}^{jk} \right\rangle \\
&= -\frac{G}{8\pi r^2 c^5} \left\langle \left( \mathcal{P}_{cj} \mathcal{P}_{dk} - \frac{1}{2} \mathcal{P}_{cd} \mathcal{P}_{jk} \right) \ddot{\mathcal{I}}^{cd} \ddot{\mathcal{I}}^{jk} \right\rangle \\
&= -\frac{G}{8\pi r^2 c^5} \left\langle \ddot{\mathcal{I}}_{ab} \ddot{\mathcal{I}}^{ab} - 2n_a n_b \ddot{\mathcal{I}}^{ac} \ddot{\mathcal{I}}^b_c + \frac{1}{2} n_a n_b n_c n_d \ddot{\mathcal{I}}^{ab} \ddot{\mathcal{I}}^{cd} \right\rangle. \tag{C.7}
\end{aligned}$$

The gravitational wave luminosity requires integration over a sphere of radius  $r \gg \lambda_{GW}$  where  $dA = r^2 d\Omega$ . Using the fact that the time average of a sum is the sum of the time averages, the GW luminosity is

$$\begin{aligned}
\mathcal{L}_{GW} &= -\frac{G}{8\pi c^5} \int d\Omega \left\langle \ddot{\mathcal{I}}_{ab} \ddot{\mathcal{I}}^{ab} - 2n_a n_b \ddot{\mathcal{I}}^{ac} \ddot{\mathcal{I}}^b_c + \frac{1}{2} n_a n_b n_c n_d \ddot{\mathcal{I}}^{ab} \ddot{\mathcal{I}}^{cd} \right\rangle \\
&= -\frac{G}{8\pi c^5} \left[ \left\langle \ddot{\mathcal{I}}_{ab} \ddot{\mathcal{I}}^{ab} \right\rangle \int d\Omega - 2 \left\langle \ddot{\mathcal{I}}^{ac} \ddot{\mathcal{I}}^b_c \right\rangle \int d\Omega n_a n_b + \frac{1}{2} \left\langle \ddot{\mathcal{I}}^{ab} \ddot{\mathcal{I}}^{cd} \right\rangle \int d\Omega n_a n_b n_c n_d \right] \\
&= -\frac{G}{8\pi c^5} \left[ 4\pi \left\langle \ddot{\mathcal{I}}_{ab} \ddot{\mathcal{I}}^{ab} \right\rangle - \frac{8\pi}{3} \delta_{ab} \left\langle \ddot{\mathcal{I}}^{ac} \ddot{\mathcal{I}}^b_c \right\rangle + \frac{2\pi}{15} (\delta_{ab} \delta_{cd} + \delta_{ac} \delta_{bd} + \delta_{ad} \delta_{bc}) \left\langle \ddot{\mathcal{I}}^{ab} \ddot{\mathcal{I}}^{cd} \right\rangle \right] \\
&= -\frac{G}{8\pi c^5} \left[ \frac{60\pi}{15} \left\langle \ddot{\mathcal{I}}_{ab} \ddot{\mathcal{I}}^{ab} \right\rangle - \frac{40\pi}{15} \left\langle \ddot{\mathcal{I}}^{ab} \ddot{\mathcal{I}}_{ab} \right\rangle + \frac{2\pi}{15} \left\langle \ddot{\mathcal{I}}^a_a \ddot{\mathcal{I}}^c_c \right\rangle + \frac{4\pi}{15} \left\langle \ddot{\mathcal{I}}^{ab} \ddot{\mathcal{I}}_{ab} \right\rangle \right] \\
&= -\frac{1}{5} \frac{G}{c^5} \left\langle \ddot{\mathcal{I}}_{ab} \ddot{\mathcal{I}}^{ab} \right\rangle, \tag{C.8}
\end{aligned}$$

where in the penultimate step one may notice  $\ddot{\mathcal{I}}^c_c = 0$  because  $\ddot{\mathcal{I}}^{ab}$  is traceless.

Similarly, it can be shown [59] that the angular momentum  $\mathbf{J}$  carried away from a system at quadrupolar order can be written as the sum of the orbital  $\mathbf{L}$  and spin  $\mathbf{S}$  angular momentum losses, i.e.  $\dot{\mathbf{J}} = \dot{\mathbf{L}} + \dot{\mathbf{S}}$ . The spin angular momentum will be zero for Schwarzschild holes and reaches a maximum for a maximally rotating Kerr black hole when the effective rotational velocity of the event horizon approaches the speed of light. Writing the losses in

each spatial direction gives

$$\begin{aligned}
\frac{dJ^a}{dt} &\equiv \frac{dL^a}{dt} + \frac{dS^a}{dt} \\
&= -\frac{2}{15} \frac{G}{c^5} \epsilon^{abc} \langle \ddot{\mathcal{I}}_{bd} \ddot{\mathcal{I}}_c^d \rangle - \frac{4}{15} \frac{G}{c^5} \epsilon^{abc} \langle \ddot{\mathcal{I}}_{bd} \ddot{\mathcal{I}}_c^d \rangle \\
&= -\frac{2}{5} \frac{G}{c^5} \epsilon^{abc} \langle \ddot{\mathcal{I}}_{bd} \ddot{\mathcal{I}}_c^d \rangle,
\end{aligned} \tag{C.9}$$

where  $\epsilon^{abc}$  is the totally antisymmetric Levi-Civita tensor in three dimensions defined as

$$\epsilon^{abc} \equiv \begin{cases} +1 & \text{for cyclic permutations of } abc \\ -1 & \text{for anticyclic permutations of } abc \\ 0 & \text{otherwise} \end{cases} . \tag{C.10}$$

# References

- [1] A. Einstein, Die formale Grundlage der allgemeinen Relativitätstheorie, Sitzungsberichte der Königlich Preußischen Akademie der Wissenschaften (Berlin), Seite 1030-1085 (1914).
- [2] A. Einstein, Zur allgemeinen Relativitätstheorie, Sitzungsberichte der Königlich Preußischen Akademie der Wissenschaften (Berlin), Seite 778-786 (1915).
- [3] A. Einstein, Erklärung der Perihelbewegung des Merkur aus der allgemeinen Relativitätstheorie, Sitzungsberichte der Königlich Preußischen Akademie der Wissenschaften (Berlin), Seite 831-839 (1915).
- [4] A. Einstein, Die Feldgleichungen der Gravitation, Sitzungsberichte der Königlich Preußischen Akademie der Wissenschaften (Berlin), Seite 844-847 (1915).
- [5] A. Einstein, Näherungsweise Integration der Feldgleichungen der Gravitation, Sitzungsberichte der Königlich Preußischen Akademie der Wissenschaften (Berlin), Seite 688-696 (1916).
- [6] J. C. Maxwell, VIII. A dynamical theory of the electromagnetic field, Phil. Trans. R. Soc. Lond. 155 (1865) 459–512. doi:10.1098/rstl.1865.0008.
- [7] A. Einstein, Zur Elektrodynamik bewegter Körper, Annalen der Physik (1905) 322 (1905) 891–921. doi:10.1002/andp.19053221004.
- [8] K. Schwarzschild, Über das Gravitationsfeld eines Massenpunktes nach der Einsteinschen Theorie, Sitzungsberichte der Königlich Preußischen Akademie der Wissenschaften (Berlin), Seite 189-196 (1916).
- [9] S. W. Hawking, Particle creation by black holes, Communications in Mathematical Physics 43 (1975) 199–220. doi:10.1007/BF02345020.
- [10] J. R. Rice, B. Zhang, Cosmological evolution of primordial black holes, Journal of High Energy Astrophysics 13 (2017) 22–31. arXiv:1702.08069, doi:10.1016/j.jheap.2017.02.002.
- [11] J. R. Rice, B. Zhang, Transient electromagnetic signatures from supermassive black hole binary coalescence, *To be submitted to ApJ (2018)*.

- [12] Y. B. Zel'dovich, I. D. Novikov, The Hypothesis of Cores Retarded during Expansion and the Hot Cosmological Model, *AZh* 43 (1966) 758.
- [13] B. J. Carr, K. Kohri, Y. Sendouda, J. Yokoyama, New cosmological constraints on primordial black holes, *Phys. Rev. D* 81 (10) (2010) 104019. [arXiv:0912.5297](#), [doi:10.1103/PhysRevD.81.104019](#).
- [14] T. N. Ukwatta, D. R. Stump, J. T. Linnemann, J. H. MacGibbon, S. S. Marinelli, T. Yapici, K. Tollefson, Primordial Black Holes: Observational characteristics of the final evaporation, *Astroparticle Physics* 80 (2016) 90–114. [arXiv:1510.04372](#), [doi:10.1016/j.astropartphys.2016.03.007](#).
- [15] B. P. Abbott, R. Abbott, T. D. Abbott, M. R. Abernathy, F. Acernese, K. Ackley, C. Adams, T. Adams, P. Addesso, R. X. Adhikari, et al., Observation of Gravitational Waves from a Binary Black Hole Merger, *Physical Review Letters* 116 (6) (2016) 061102. [arXiv:1602.03837](#), [doi:10.1103/PhysRevLett.116.061102](#).
- [16] B. P. Abbott, et al., Gw151226: Observation of gravitational waves from a 22-solar-mass binary black hole coalescence, *Phys. Rev. Lett.* 116 (2016) 241103. [doi:10.1103/PhysRevLett.116.241103](#).  
URL <https://link.aps.org/doi/10.1103/PhysRevLett.116.241103>
- [17] B. P. Abbott, et al., Gw170104: Observation of a 50-solar-mass binary black hole coalescence at redshift 0.2, *Phys. Rev. Lett.* 118 (2017) 221101. [doi:10.1103/PhysRevLett.118.221101](#).  
URL <https://link.aps.org/doi/10.1103/PhysRevLett.118.221101>
- [18] B. P. Abbott, R. Abbott, T. D. Abbott, F. Acernese, K. Ackley, C. Adams, T. Adams, P. Addesso, R. X. Adhikari, V. B. Adya, et al., GW170608: Observation of a 19 Solar-mass Binary Black Hole Coalescence, *ApJ* 851 (2017) L35. [arXiv:1711.05578](#), [doi:10.3847/2041-8213/aa9f0c](#).
- [19] B. P. Abbott, et al., Gw170814: A three-detector observation of gravitational waves from a binary black hole coalescence, *Phys. Rev. Lett.* 119 (2017) 141101. [doi:10.1103/PhysRevLett.119.141101](#).  
URL <https://link.aps.org/doi/10.1103/PhysRevLett.119.141101>
- [20] V. Connaughton, E. Burns, A. Goldstein, L. Blackburn, M. S. Briggs, B.-B. Zhang, J. Camp, N. Christensen, C. M. Hui, P. Jenke, T. Littenberg, J. E. McEnery, J. Racusin, P. Shawhan, L. Singer, J. Veitch, C. A. Wilson-Hodge, P. N. Bhat, E. Bissaldi, W. Cleveland, G. Fitzpatrick, M. M. Giles, M. H. Gibby, A. von Kienlin, R. M. Kippen, S. McBreen, B. Mailyan, C. A. Meegan, W. S. Paciesas, R. D. Preece, O. J. Roberts, L. Sparke, M. Stanbro, K. Toelge, P. Veres, Fermi GBM Observations of LIGO Gravitational-wave Event GW150914, *ApJ* 826 (2016) L6. [arXiv:1602.03920](#), [doi:10.3847/2041-8205/826/1/L6](#).

- [21] B. J. Carr, K. Kohri, Y. Sendouda, J. Yokoyama, Constraints on primordial black holes from the Galactic gamma-ray background, *Phys. Rev. D* 94 (4) (2016) 044029. [arXiv:1604.05349](https://arxiv.org/abs/1604.05349), [doi:10.1103/PhysRevD.94.044029](https://doi.org/10.1103/PhysRevD.94.044029).
- [22] K. J. Mack, J. P. Ostriker, M. Ricotti, Growth of Structure Seeded by Primordial Black Holes, *ApJ* 665 (2007) 1277–1287. [arXiv:astro-ph/0608642](https://arxiv.org/abs/astro-ph/0608642), [doi:10.1086/518998](https://doi.org/10.1086/518998).
- [23] M. Ricotti, J. P. Ostriker, K. J. Mack, Effect of Primordial Black Holes on the Cosmic Microwave Background and Cosmological Parameter Estimates, *ApJ* 680 (2008) 829–845. [arXiv:0709.0524](https://arxiv.org/abs/0709.0524), [doi:10.1086/587831](https://doi.org/10.1086/587831).
- [24] T. N. Ukwatta, K. Hurley, J. H. MacGibbon, D. S. Svinkin, R. L. Aptekar, S. V. Golenetskii, D. D. Frederiks, V. D. Pal'shin, J. Goldsten, W. Boynton, A. S. Kozyrev, A. Rau, A. von Kienlin, X. Zhang, V. Connaughton, K. Yamaoka, M. Ohno, N. Ohmori, M. Feroci, F. Frontera, C. Guidorzi, T. Cline, N. Gehrels, H. A. Krimm, J. McTiernan, Investigation of Primordial Black Hole Bursts Using Interplanetary Network Gamma-ray Bursts, *ApJ* 826 (2016) 98. [arXiv:1512.01264](https://arxiv.org/abs/1512.01264), [doi:10.3847/0004-637X/826/1/98](https://doi.org/10.3847/0004-637X/826/1/98).
- [25] Planck Collaboration, P. A. R. Ade, N. Aghanim, M. Arnaud, M. Ashdown, J. Aumont, C. Baccigalupi, A. J. Banday, R. B. Barreiro, J. G. Bartlett, et al., Planck 2015 results. XIII. Cosmological parameters (2015), *ArXiv e-prints* [arXiv:1502.01589](https://arxiv.org/abs/1502.01589).
- [26] A. Friedmann, Über die Krümmung des Raumes, *Zeitschrift für Physik* 10 (1922) 377–386. [doi:10.1007/BF01332580](https://doi.org/10.1007/BF01332580).
- [27] S. W. Hawking, G. F. R. Ellis, *The large-scale structure of space-time.*, Cambridge University Press, Cambridge (UK), 1973, <http://adsabs.harvard.edu/abs/1973lsss.book.....H>.
- [28] E. W. Kolb, M. S. Turner, *The early universe.*, Addison-Wesley, Redwood City, CA, 1990, <http://adsabs.harvard.edu/abs/1990eaun.book.....K>.
- [29] G. Jungman, M. Kamionkowski, K. Griest, Supersymmetric dark matter, *Phys. Rep.* 267 (1996) 195–373. [arXiv:hep-ph/9506380](https://arxiv.org/abs/hep-ph/9506380), [doi:10.1016/0370-1573\(95\)00058-5](https://doi.org/10.1016/0370-1573(95)00058-5).
- [30] K. A. Olive, Particle Data Group, Review of Particle Physics, *Chinese Physics C* 38 (9) (2014) 090001. [doi:10.1088/1674-1137/38/9/090001](https://doi.org/10.1088/1674-1137/38/9/090001).
- [31] S. Gupta, X. Luo, B. Mohanty, H. G. Ritter, N. Xu, Scale for the Phase Diagram of Quantum Chromodynamics, *Science* 332 (2011) 1525. [arXiv:1105.3934](https://arxiv.org/abs/1105.3934), [doi:10.1126/science.1204621](https://doi.org/10.1126/science.1204621).
- [32] D. J. Fixsen, The Temperature of the Cosmic Microwave Background, *ApJ* 707 (2009) 916–920. [arXiv:0911.1955](https://arxiv.org/abs/0911.1955), [doi:10.1088/0004-637X/707/2/916](https://doi.org/10.1088/0004-637X/707/2/916).
- [33] P. J. E. Peebles, *Principles of Physical Cosmology*, Princeton University Press, Princeton, NJ, 1993, <http://adsabs.harvard.edu/abs/1993ppc..book.....P>.

- [34] J. L. Feng, Dark Matter Candidates from Particle Physics and Methods of Detection, *ARA&A* 48 (2010) 495–545. [arXiv:1003.0904](#), [doi:10.1146/annurev-astro-082708-101659](#).
- [35] G. N. Remmen, S. M. Carroll, How many e-folds should we expect from high-scale inflation?, *Phys. Rev. D* 90 (6) (2014) 063517. [arXiv:1405.5538](#), [doi:10.1103/PhysRevD.90.063517](#).
- [36] J. H. MacGibbon, Quark- and gluon-jet emission from primordial black holes. II. The emission over the black-hole lifetime, *Phys. Rev. D* 44 (1991) 376–392. [doi:10.1103/PhysRevD.44.376](#).
- [37] D. N. Page, Particle emission rates from a black hole: Massless particles from an uncharged, nonrotating hole, *Phys. Rev. D* 13 (1976) 198–206. [doi:10.1103/PhysRevD.13.198](#).
- [38] J. R. Primack, *Cosmological Structure Formation*, ArXiv e-prints (2015)[arXiv:1505.02821](#).
- [39] H. Mo, F. C. van den Bosch, S. White, *Galaxy Formation and Evolution*, Cambridge University Press, Cambridge, UK, 2010, <http://adsabs.harvard.edu/abs/2010gfe..book....M>.
- [40] H. Bondi, On spherically symmetrical accretion, *MNRAS* 112 (1952) 195. [doi:10.1093/mnras/112.2.195](#).
- [41] B. J. Carr, Pregalactic black hole accretion and the thermal history of the universe, *MNRAS* 194 (1981) 639–668. [doi:10.1093/mnras/194.3.639](#).
- [42] X.-B. Wu, F. Wang, X. Fan, W. Yi, W. Zuo, F. Bian, L. Jiang, I. D. McGreer, R. Wang, J. Yang, Q. Yang, D. Thompson, Y. Beletsky, An ultraluminous quasar with a twelve-billion-solar-mass black hole at redshift 6.30, *Nature* 518 (2015) 512–515. [arXiv:1502.07418](#), [doi:10.1038/nature14241](#).
- [43] B. P. Abbott, R. Abbott, T. D. Abbott, M. R. Abernathy, F. Acernese, K. Ackley, C. Adams, T. Adams, P. Addesso, R. X. Adhikari, et al., Observation of Gravitational Waves from a Binary Black Hole Merger, *Physical Review Letters* 116 (6) (2016) 061102. [arXiv:1602.03837](#), [doi:10.1103/PhysRevLett.116.061102](#).
- [44] B. P. Abbott, R. Abbott, T. D. Abbott, M. R. Abernathy, F. Acernese, K. Ackley, C. Adams, T. Adams, P. Addesso, R. X. Adhikari, et al., GW151226: Observation of Gravitational Waves from a 22-Solar-Mass Binary Black Hole Coalescence, *Physical Review Letters* 116 (24) (2016) 241103. [arXiv:1606.04855](#), [doi:10.1103/PhysRevLett.116.241103](#).
- [45] M. Sasaki, T. Suyama, T. Tanaka, S. Yokoyama, Primordial Black Hole Scenario for the Gravitational-Wave Event GW150914, *Physical Review Letters* 117 (6) (2016) 061101. [arXiv:1603.08338](#), [doi:10.1103/PhysRevLett.117.061101](#).

- [46] L. Chen, Q.-G. Huang, K. Wang, Constraint on the abundance of primordial black holes in dark matter from Planck data, *J. Cosmology Astropart. Phys.* 12 (2016) 044. [arXiv:1608.02174](#), [doi:10.1088/1475-7516/2016/12/044](#).
- [47] B. Horowitz, Revisiting Primordial Black Holes Constraints from Ionization History, *ArXiv e-prints* (2016)[arXiv:1612.07264](#).
- [48] Y. Ali-Haïmoud, M. Kamionkowski, Cosmic microwave background limits on accreting primordial black holes, *Phys. Rev. D* 95 (4) (2017) 043534. [arXiv:1612.05644](#), [doi:10.1103/PhysRevD.95.043534](#).
- [49] S. A. Hughes, Gravitational Waves from Merging Compact Binaries, *ARA&A* 47 (2009) 107–157. [arXiv:0903.4877](#), [doi:10.1146/annurev-astro-082708-101711](#).
- [50] L.-X. Li, B. Paczyński, Transient Events from Neutron Star Mergers, *ApJ* 507 (1998) L59–L62. [arXiv:astro-ph/9807272](#), [doi:10.1086/311680](#).
- [51] D. Alic, P. Moesta, L. Rezzolla, O. Zanotti, J. L. Jaramillo, Accurate Simulations of Binary Black Hole Mergers in Force-free Electrodynamics, *ApJ* 754 (2012) 36. [arXiv:1204.2226](#), [doi:10.1088/0004-637X/754/1/36](#).
- [52] P. Mösta, C. Palenzuela, L. Rezzolla, L. Lehner, S. Yoshida, D. Pollney, Vacuum electromagnetic counterparts of binary black-hole mergers, *Phys. Rev. D* 81 (6) (2010) 064017. [arXiv:0912.2330](#), [doi:10.1103/PhysRevD.81.064017](#).
- [53] P. Mösta, C. Palenzuela, L. Rezzolla, L. Lehner, S. Yoshida, D. Pollney, Vacuum electromagnetic counterparts of binary black-hole mergers, *Phys. Rev. D* 81 (2010) 064017. [doi:10.1103/PhysRevD.81.064017](#).  
URL <https://link.aps.org/doi/10.1103/PhysRevD.81.064017>
- [54] C. Palenzuela, L. Lehner, S. Yoshida, Understanding possible electromagnetic counterparts to loud gravitational wave events: Binary black hole effects on electromagnetic fields, *Phys. Rev. D* 81 (2010) 084007. [doi:10.1103/PhysRevD.81.084007](#).  
URL <https://link.aps.org/doi/10.1103/PhysRevD.81.084007>
- [55] A. Einstein, Zur Elektrodynamik bewegter Körper, *Annalen der Physik* 322 (1905) 891–921. [doi:10.1002/andp.19053221004](#).
- [56] H. Minkowski, Die Grundgleichungen für die elektromagnetischen Vorgänge in bewegten Körpern, *Nachrichten von der Gesellschaft der Wissenschaften zu Göttingen, Mathematisch-Physikalische Klasse*, 1908, Seite 53-111.
- [57] C. W. Misner, K. S. Thorne, J. A. Wheeler, *Gravitation*, W.H. Freeman and Co., San Francisco, CA, 1973.
- [58] J. L. Synge, A. Schild, *Tensor calculus*, University of Toronto Press, Toronto, Canada, 1949.

- [59] M. Maggiore, *Gravitational waves volume 1: theory and experiments*, Oxford University Press Inc., New York, NY, 2008.
- [60] P. C. Peters, J. Mathews, Gravitational Radiation from Point Masses in a Keplerian Orbit, *Physical Review* 131 (1963) 435–440. doi:10.1103/PhysRev.131.435.
- [61] P. C. Peters, Gravitational Radiation and the Motion of Two Point Masses, *Physical Review* 136 (1964) 1224–1232. doi:10.1103/PhysRev.136.B1224.
- [62] J. Creighton, W. Anderson, *Gravitational-Wave Physics and Astronomy: An Introduction to Theory, Experiment and Data Analysis.*, Wiley-VCH, Weinheim, Germany, 2011.
- [63] T. Dal Canton, et al., Implementing a search for aligned-spin neutron star-black hole systems with advanced ground based gravitational wave detectors, *Phys. Rev. D* 90 (8) (2014) 082004. arXiv:1405.6731, doi:10.1103/PhysRevD.90.082004.
- [64] S. A. Usman, et al., The PyCBC search for gravitational waves from compact binary coalescence, *Class. Quant. Grav.* 33 (21) (2016) 215004. arXiv:1508.02357, doi:10.1088/0264-9381/33/21/215004.
- [65] A. H. Nitz, T. Dent, T. Dal Canton, S. Fairhurst, D. A. Brown, Detecting binary compact-object mergers with gravitational waves: Understanding and Improving the sensitivity of the PyCBC search, *Astrophys. J.* 849 (2) (2017) 118. arXiv:1705.01513, doi:10.3847/1538-4357/aa8f50.
- [66] D. Neilsen, L. Lehner, C. Palenzuela, E. W. Hirschmann, S. L. Liebling, P. M. Motl, T. Garrett, Boosting jet power in black hole spacetimes, *Proceedings of the National Academy of Science* 108 (2011) 12641–12646. arXiv:1012.5661, doi:10.1073/pnas.1019618108.
- [67] G. B. Rybicki, A. P. Lightman, *Radiative processes in astrophysics*, Wiley-Interscience, 1979.
- [68] K. C. Westfold, The Polarization of Synchrotron Radiation., *ApJ* 130 (1959) 241. doi:10.1086/146713.
- [69] A. G. Pacholczyk, *Radio astrophysics. Nonthermal processes in galactic and extragalactic sources*, Freeman, San Francisco, CA, 1970.
- [70] B. Zhang, *The physics of gamma-ray bursts*, Cambridge University Press, Cambridge, UK, 2018.

# Curriculum Vitae

## JARED ROBERT RICE

E-mail: [jared.r.rice@protonmail.ch](mailto:jared.r.rice@protonmail.ch)

Website: <http://www.physics.unlv.edu/~jrice/>

### Education

---

PhD, Astronomy expected May 2018

University of Nevada, Las Vegas

Advisor: *Bing Zhang, PhD*

MS, Physics, 2012

Montana State University

Advisors: *Sachiko Tsuruta, PhD and Jiong Qiu, PhD*

BS, Astrophysics, 2008

University of California, Santa Cruz

Advisor: *Joel Primack, PhD*

### Research interests

---

- Electromagnetic counterparts of binary compact object mergers
  - EM radiation mechanisms, relativistic blast waves, evolving synchrotron spectra, interaction of EM fields with gravitational waves, predicting observational signatures of EM signals
- Very long baseline interferometry of supermassive black hole jet cores
  - Probing black hole environments using the frequency-dependent synchrotron radio emission, utilizing the Very Long Baseline Array for astrometry of jet cores
- Primordial black holes
  - Accretion and evaporation histories of PBHs, importance of PBHs as cosmic messengers

### Publications

---

**Numerics:** Total citations: **9**, h-index: **2**, First author h-index: **1**

1. **Rice, J.R.** and Zhang, B., *Radio afterglow of inspiral-driven plasma waves in supermassive black hole binary mergers*, (to be submitted to ApJ, 2018)
2. **Rice, J.R.**, Zavala, R.T., and Taylor, G.B., *Core shifts in compact symmetric objects*, (in progress, 2018)
3. **Rice, J.R.** and Zhang, B., *Cosmological evolution of primordial black holes*, Journal of High Energy Astrophysics, **13**, 22 (2017)

4. Lü, H.-J., Zhang, H.-M., Zhong, S.-Q., Hou, S.-J., Sun, H., **Rice, J.R.**, and Liang, E.-W., *Magnetar central engine and possible gravitational wave emission of nearby short GRB 160821B* *Astrophysical Journal*, **835**, 181 (2017)
5. Li, L.B., Zhang, Z.B., and **Rice, J.R.**, *Radio afterglow rebrightening: evidence for multiple active phases in gamma-ray burst central engines*, *Astrophysics and Space Science*, **359**, 37 (2015)

#### *Textbook editing and illustrations*

---

- Copyedited and produced numerous figures for Bing Zhang, PhD, *The Physics of Gamma-Ray Bursts*, Cambridge University Press (2018)
- Produced various diagrams for Thomas Banks, PhD, *Modern Quantum Field Theory: A Concise Introduction*, Cambridge University Press (2008)

#### *Awards*

---

- NASA Space Grant Consortium Graduate Research Fellowship (2016) \$ 10,500
- UNLV Foundation Bigelow Travel Grant (2014) \$ 4,000
- NSF REU Research Grant (2007) \$ 5,000
- UCSC Crown College Undergraduate Research Fellowship (2007) \$ 700
- MSU Excellent Graduate Teaching Assistant Award

#### *Skills*

---

- Python and iPython
  - Developed synchrotron radiation code for blast wave afterglow calculations
  - Developed cosmology-dependent primordial black hole accretion and evaporation code
- VLBA data reduction using the Astronomical Image Processing System (*AIPS*) code.
- PhD focus: electromagnetic counterparts of gravitational wave events, relativistic blast waves, primordial black holes, and high energy astrophysical synchrotron sources.

#### *Teaching*

---

- Adjunct Instructor of Physics (2012/2013), Miami University, Oxford, OH
- Adjunct Instructor of Physics (2013), Miami University Hamilton, Hamilton, OH
- Graduate Teaching Assistant (2013 – 2018), UNLV
- Graduate Teaching Assistant (2009 – 2012), MSU
- Guest lecturer, Solar System Astronomy (Fall 2011), MSU

#### *Conferences & Workshops*

---

- LIGO Open Data Workshop # 1, Caltech, Pasadena, CA, March 25–27, 2018
- 16th Synthesis Imaging Workshop, New Mexico Tech, Socorro, NM, May 16–23, 2018
  - Will attend.
- IAU 338: GW Astrophysics: Early Results from GW Searches and EM Counterparts, 2017
  - Contributed talk: “Radio afterglow of gravitation-driven plasma waves in SMBH binary mergers”

- Eighth Huntsville Gamma-Ray Burst Symposium, 2016
  - Poster: “*Cosmological evolution of primordial black holes*”
- UNLV/Caltech Radio Transient Workshop, Las Vegas, 2016
- UNLV Gamma-Ray Bursts and Numerical Simulations Workshop, Las Vegas, 2015
- European Week of Astronomy and Space Science; Geneva, Switzerland, 2014
- IAU 307: New Windows on Massive Stars; Geneva, Switzerland, 2014
- UCSC Galaxy Formation and Evolution Workshop; Santa Cruz, 2007
- All-Wavelength Extended Groth Strip International Survey Meeting; Santa Cruz, 2006

### *Outreach*

---

- Visiting Outreach Astronomer (2017 – present) in Nipton, CA
- Astronomy Day Volunteer (2010 – 2012), Museum of the Rockies, Bozeman, MT
- Instructor, Rocket Physics (2011), *MSU Peaks & Potentials* (elementary students)

### *Professional references*

---

1. Bing Zhang, PhD, Professor of Astrophysics, UNLV
  - E-mail: [zhang@physics.unlv.edu](mailto:zhang@physics.unlv.edu)
  - Phone: +1 702/895-4050
  - Website: <http://www.physics.unlv.edu/~bzhang/>
2. Robert Zavala, PhD, Astronomer, United States Naval Observatory, Flagstaff Station
  - E-mail: [bzavala@nofs.navy.mil](mailto:bzavala@nofs.navy.mil)
  - Phone: +1 928/779-5132 (260)
  - Website: <http://www.nofs.navy.mil/>
3. Darrell Pepper, PhD, Professor of Mechanical Engineering, UNLV
  - E-mail: [darrell.pepper@unlv.edu](mailto:darrell.pepper@unlv.edu)
  - Phone: +1 702/895-1056
  - Website: [http://ncacm.unlv.edu/HTML/staff/faculty/pepper/faculty\\_pepper.html](http://ncacm.unlv.edu/HTML/staff/faculty/pepper/faculty_pepper.html)

